UCLouvain

AGRO LOUVAIN

Faculté des bioingénieurs

Oxidative cleavage of oleic acid with alumina-ruthenium composites

Auteur : Odile Malburny
Promoteur(s) : Eric Gaigneaux (UCLouvain)
Co-promoteur : Sebastián Antonio Gámez Rivera (UCLouvain)
Lecteur(s) : Sophie Hermans (UCLouvain) et Damien Debecker(UCLouvai)
Année académique 2021-2022
Mémoire de fin d'études présenté en vue de l'obtention du diplôme de Bioingénieur : Chimie et bioindustries

Acknowledgments

D'abord, je souhaiterais remercier mon promoteur, le professeur Eric Gaigneaux, pour son accompagnement et de m'avoir soutenue bien avant le début de ce mémoire. C'est l'une des personnes les plus humaines que j'ai rencontrées. Merci pour tout.

Je souhaiterais aussi remercier Sebastian Gamez pour m'avoir accompagnée lors de mes manipulations, lors du traitement de mes données, pour m'avoir soutenue et pour **sa patience** lors des relectures.

Je souhaiterais également remercier François Devred, pour m'avoir expliqué le fonctionnement des machines, pour m'avoir aidée à comprendre certains de mes résultats, pour m'avoir aidée à adopter un comportement professionnel au laboratoire (Work in progress), pour sa franchise, sa bonne humeur et sa patience.

Merci à Valentin Smeets, qui est la meilleure personne que ce soit humainement ou scientifiquement que j'ai rencontrée à ce jour. Il était la première personne vers qui je me tournais dès que j'avais un problème au laboratoire.

Merci à Alixandre Magerat pour son soutien, pour m'avoir aidée lors de manipulations et pour avoir corrigé mes fautes d'orthographe.

Je souhaiterais également remercier le professeur Patrick Gerin qui m'a permis d'utiliser les laboratoires du GEBI pendant une partie de mes manipulations. Un grand merci à Thomas Nicolay pour son soutien technique mais aussi pour les bons moments. (Merci d'être venu me libérer lorsque que j'avais réussi à m'enfermer dehors sur les balcons du GEBI.)

Merci à Fanny Hanon, Nadia Gholampour, Margot Van der Verren, Tommy Haynes de m'avoir aidée quand j'avais des problèmes avec les machines.

Merci à tous les membres du Lavoisier C.03 pour m'avoir aidée ou supportée.

Je tiens aussi à remercier les professeurs Sophie Hermans et Damien Debecker d'avoir accepté de lire ce mémoire et d'assister à ma défense orale.

De manière plus personnelle, je veux remercier Dominique Gérard, ma maman, pour m'avoir soutenue émotionnellement durant ce mémoire et de m'avoir écouté parler de celui-ci alors qu'elle n'a aucune notion de chimie. Finalement, merci à mes co-koteurs (en particulier Clara Lens) qui ont accepté la mission de me réveiller à chaque fois que j'avais une manipulation ou une présentation au matin. Sans eux, ce mémoire n'aurait pas été possible.

Tables of contents

1 State of the art

1.1 Context

Since the last century petrochemical raw materials have been used for the production of adhesives, cosmetics, fertilizers, paint , rubbers, polymers among other industrial products [1].Unfortunately petrochemical stocks are shrinking. In addition, they are toxic and polluting[2].On the other hand, oils and fats are promising renewable feedstocks because they are abundant in nature, biodegradable and they are not toxic. These renewable raw materials are mainly formed of triglycerides (Figure 1) which consist of a glycerol molecule with three fatty acids. The latter, also known as fatty acids, are long hydrocarbon chains with a carboxylic acid site and possible olefinic bonds. Fatty acids are called saturated when they do not contain a carbon-carbon double bond (unsaturation) and unsaturated fatty acids (UFAs) when they possess one or more olefinic bonds. Fatty acids from animal fats are mostly composed by saturated fatty acids and those from vegetable oils are mostly unsaturated[2].The decomposition of triglycerides releases fatty acids which may evolve into fatty acid methyl esters, fatty amines or fatty alcohols[2].There are two functional groups which can be exploited in UFAs : the double bond and the acidic group. Most of the industrial applications use the carboxylic group as a reactive site to carry out further reactions while only 10 % of the industrial reactions are involved with the carbon-carbon double bond (unsaturation)[2].

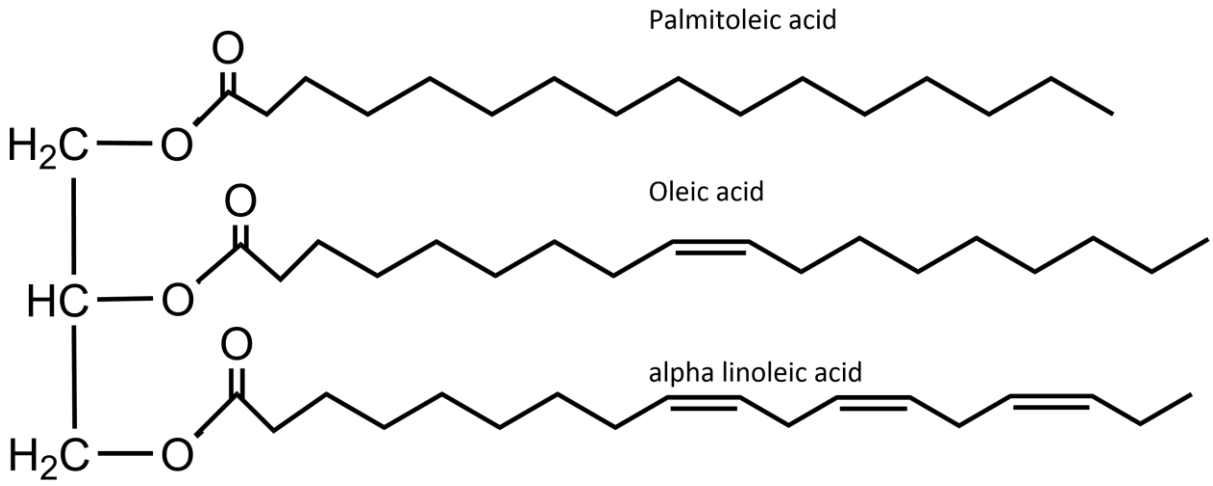

Figure 1:Structure of a given triglyceride.

In this regard, epoxidation and hydrogenation reactions are the most common examples involving olefinic bonds. For instance, the epoxidation of oleic acid at an industrial scale is produced by the Prileshajev epoxidation procedure which uses a peracid (O_3) to

transfer its oxygen to the double bonds[3].At industrial level, the hydrogenation of oleic acid, uses Cu-Cr based catalysts at 250-350°C and 10-20 MPa[4].

In this work, the oxidative cleavage of the carbon-carbon double bonds from UFAs has been explored since it is possible to obtain high value products from cheap feedstock and because this reaction has been less documented in literature. Most of the works published so far employ homogeneous catalysts to perform this kind of reaction but they are not applicable at industrial scale. On the other hand, heterogeneous catalysts have been scarcely explored because of their poor results obtained in this regard. Diffusional issues and poor contact are just some of the few reasons why heterogeneous catalysis remains underdeveloped in the oxidative cleavage of UFAs[2].To propose an alternative, herein we propose a new catalytic system based on the functionalization of alumina with polydopamine (a polymer coating) towards the heterogenization of Ru. In combination with a strong oxidizing agent (e.g. $NaIO_4$) the heterogeneous catalyst can produce RuO_4, the active species responsible for the scission of the carbon-carbon double bonds in UFAs and the corresponding production of carboxylic and dicarboxylic acids[5].

1.2 Oxidative cleavage of UFAs

Oxidative cleavage corresponds to the rupture of carbon-carbon double bonds and the formation of different carbonyl compounds. Different products are therefore possible as alcohols, aldehydes, ketones or carboxylic acids[2]. Most of the examples related to this reaction use oleic acid (OA),formerly called cis-9-octadecenoic acid, because it is the most abundant mono-UFA. OA can be found in olive, pecan, peanut, macadamia, sunflower, grape seed, rapeseed or in animal fats such as chicken, turkey and lard. As shown in Figure 2, oleic acid gives a ratio of one mole of azelaic acid (AA), $HOOC(CH_2)_7COOH$, for one mole of pelargonic acid(PA), $HOOC(CH_2)_7CH_3$, through its oxidation. Both oxidative cleavage products can be used in several applications. For instance, azelaic acid is used in the pharmaceutical, cosmetic and polymers industry. It can also serve as a lubricant or as a plasticizer. In fact, the market size of azelaic acid is expected to reach 140 million USD by 2025 [6].On the other hand, pelargonic acid is mainly used in pesticides and herbicides[6].

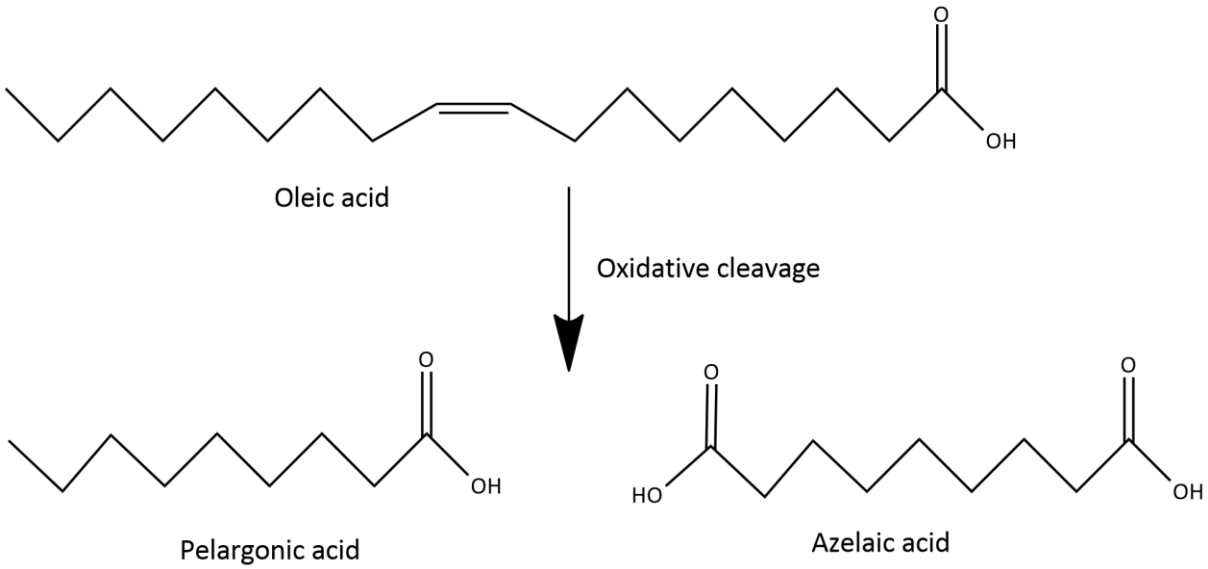

Figure 2: Oxidative cleavage of oleic acid into pelargonic acid and azelaic acid. Inspired from[7]

Oxidative cleavage of oleic acid is usually performed by ozonolysis. Ozone(O_3) can be added to carbon-carbon double bonds and then the ozonide is split by oxidation with ozone-free oxygen to form azelaic and pelargonic acids followed by a purification process[8]. This process possesses several drawbacks such as the risk of explosivity and toxicity. It is also highly energy demanding and requires sophisticated equipment[2].

On the other hand, osmium and ruthenium have attracted the attention for the oxidation of unsaturated hydrocarbons because these transition metals are quite active in this reaction.[2] As regards Ru, it is known that RuO_4 is quite active in this reaction showing a better selectivity than osmium (OsO_4). Actually, the latter tends to form undesirable intermediates such as diols. Moreover, osmium is more toxic than ruthenium[2].

With this in mind, the next section presents some examples of ruthenium in the oxidative cleavage of UFAs.

1.3 Ruthenium in the oxidative cleavage of UFAs

In homogeneous catalysis, ruthenium is initially present in the reaction medium in the form of $RuCl_3$ or RuO_2. Nevertheless, RuO_4 is the active species and therefore $RuCl_3$ or RuO_2 need to undergo an oxidation by means of a strong oxidizing agent such as $NaIO_4$. According to literature, the mechanism presented in Figure 3 begins with the coordination of RuO_4 and the UFA to form a metal-diester. The metal-dioxyethane is formed via a [3+2] pericyclic reaction. After hydrolysis, a diol is formed with consequent reduction of RuO_4 to RuO_2. The diol is cleaved by $NaIO_4$ yielding two carbonyl products (mainly aldehydes). To complete the cycle RuO_2 is re-oxidized to RuO_4 by means of $NaIO_4$[9]. The aldehyde which is formed can either be oxidized by RuO_4 or by $NaIO_4$.

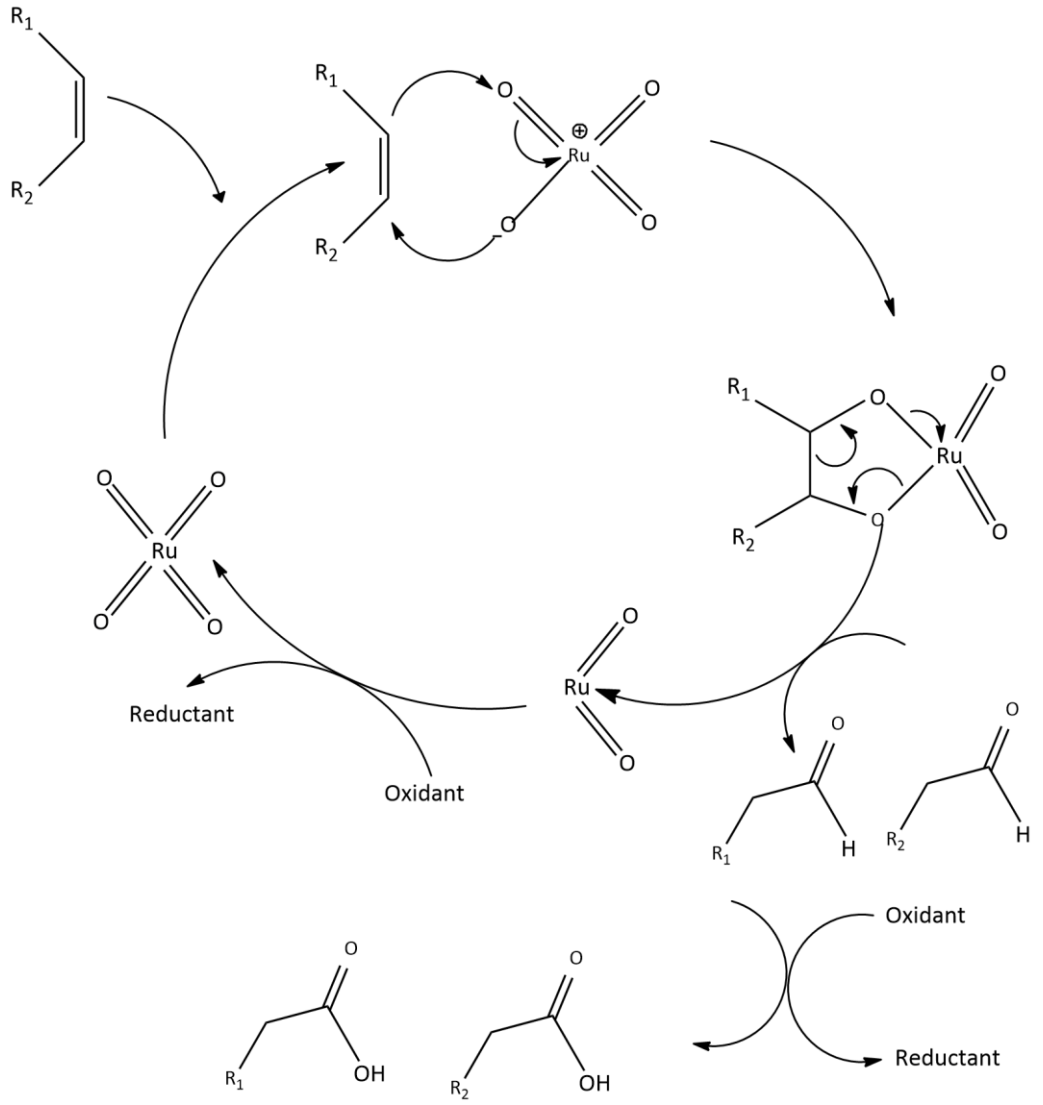

Figure 3:Mechanism of the oxidative cleavage of an alkene catalyzed by ruthenium tetroxide in the homogeneous phase.

1.4 Homogeneous catalysis using ruthenium in the oxidative cleavage of UFAs

Most of the works related to the oxidative cleavage of UFAs with Ru belong to homogeneous catalysis[5].For instance, Flogia and co-workers[10]performed the oxidative cleavage of potassium oleate with RuO_2 and NaClO as a second oxidant. RuO_2 was oxidized *in situ* into RuO_4 by NaClO. The potassium oleate was soluble in water and its oxidation was conducted in aqueous solution. The ruthenium dioxide is insoluble in aqueous solutions unlike potassium oleate so it can be recovered by filtration and reused. The conversion was complete and the yield of azelaic acid was 94%. The addition of NaOH was mandatory to keep the solution at pH 10. The active species is RuO_4 and the addition of NaOH transform RuO_2 into RuO_4 [10].

Zimmerman's and co-workers used the catalytic ruthenium system (2.2% $RuCl_3$, 4.1 eq. $NaIO_4$ solvent H_2O/MeCN/CCl_4 in ratio of (3/2/2) developed by Sharpless and co-workers with the replacement of the toxic CCl_4 with ethyl acetate (AcOEt) as organic solvent. They compare

3 solvents resistant to oxidation: ethyl acetate, acetone and cyclohexane. They found that (H_2O/MeCN/AcOEt) in ratio of (3/2/2) was the best option to obtain yield of 73% for the azelaic acid[11].

Rup *et al* used RuO_4 for the oxidative cleavage of oleic acid under ultrasonic irradiation. When ultrasound and aliquat ®336 were combined, a complete oxidative cleavage of oleic acid took place with azelaic yield of 62% and pelargonic acid yield of 99%. They also find that with a mixture of solvent of (H_2O/AcOEt, ratio 1/1) 9,10-dioxostearic acid was produced as intermediate [12].

In order to make the oxidative cleavage reaction greener, Behr *et al* used the [Ru(2,6-dipicolinate)$_2$] complex with hydrogen peroxide instead of $NaIO_4$. The solvent was a mixture of water and alcohol. The reaction was performed at 80°C for 24 hours. The yield of PA was 59%, which is significantly lower than the yield obtained by Rup *et al*. These results are ascribed to the higher number of side reactions found in the catalytic tests performed by Behr *et al* [13].

1.5 Heterogenous catalysis using ruthenium in the oxidative cleavage of UFAs

The major interest in using solid catalysts in liquid phase reaction is the possibility of recovering the active species after the reaction ends to reuse it. As regards reactions with oils and fats, limited research on heterogeneous catalysis is found in the literature. This is mainly due to poor results of this approach in terms of conversion and selectivity because of the poor contact between the substrates and the solid catalyst[2].

Nevertheless, few examples are targeted to the oxidative cleavage of UFAs. For instance, Ho *et al*. report the oxidative cleavage of methyl oleate with Ru nanoparticles immobilized on hydroxyapatite. The Zimmerman's solvent system (H_2O/MeCN/AcOEt) and $NaIO_4$ were used and led to conversions around 12% with 84% of yield for PA [14].

The oxidative cleavage of 9,10-dihydroxystearic acid methyl ester was also achieved with a $Ru(OH)_x/\gamma$-Al_2O_3 solid catalyst. The reaction was carried out under O_2 atmosphere in H_2O at 130 °C for 5 hours. The yields of PA and AA were 45 % and 43% respectively. In the recycling tests, a drop of activity after four runs was observed due to adsorption of by-products at the surface of the catalyst[15].

Papafotiou and co-workers[16],have designed a catalyst for the oxidation of various olefins. A biomimetic [Ru-(2,2';6',2"-terpyridine)-(2,2'-bipyridine)$_2$](Cl)$_2$ complex was attached to silica by aminopropyl functionalization of the silica surface then amide coupling to a bipyridine carboxylic acid and after complexation with Ru-(2,2';6',2"-terpyridine)Cl_3, tert-butylhydroperoxide was used as oxidant and tert-BuOH was used as organic phase. The reaction was carried out under air. The yield obtained with the heterogenous catalyst was compared to its analogous homogenous catalyst. The oxidation of cyclohexene, cyclooctene and cis-stilbene presented higher yields in the case of heterogenous system. The grafting process preserved the catalytic activity and may also in some cases increase its reactivity.

Following the idea of anchoring ruthenium on suitable surface support [17] , the use of a polymer coating to functionalize a macroporous alumina will be examined to anchor Ru for the synthesis of a new heterogeneous catalyst suitable for the oxidative cleavage of UFAs. Therefore, we proposed to use polydopamine (PDA), a natural coating found in nature such as mussels, able to chelate several metal cations like Ru. The chelating ability of PDA is related to the capacity of mussels to adhere to any surface under water. The study of mussel foot proteins shows an important concentration of 3,4-dihydroxy-L-phenylamine so called dopamine (DA)[18] [19]. Lee et al have reported a facile approach to surface modification in which self-polymerization of dopamine for the production of an adherent polydopamine(PDA)coating on a wide variety of materials[20]. The chemical structure of PDA presents a catechol and amine groups (Figure 4) which can form complexes with several transition metals.

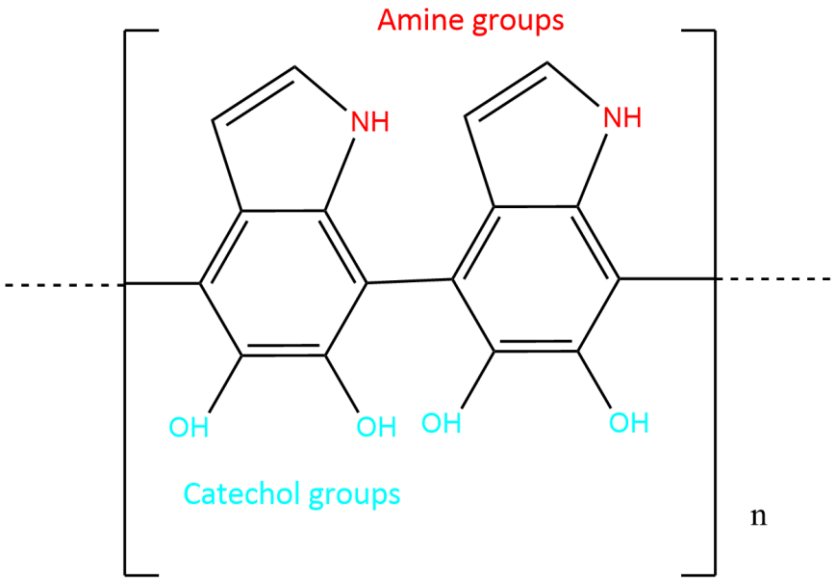

Figure 4: Linear representation of polydopamine and its functional groups

Herein, the main characteristics of this novel polymer coating are detailed.

1.6 General aspects of polydopamine and its polymerization

It is well known that the adhesion of PDA to virtually all types of surfaces is one of its best interesting properties. However, up to now, the exact adhesion mechanism remains elusive. This arises from the lack of understanding of the polymerization mechanism which is controversial. Understanding the polymerization of PDA can provide valuable data on how this polymer can interact with several materials or transition metals for catalytic applications. Several models of the polymerization of dopamine have been proposed. The different pathways give rise to different theorical structure of polydopamine. The first proposed model explained that the polymer is formed by 5,6-dihydroxyindole(DHI) units linked between each other[20]. A presentation of some models is reported below (Figure 5).

As shown in Figure 5, the 5,6-dihydroxyindole can either follow the physical self-assembly pathways to create a physical polymer or undergo the covalent oxidative polymerization route to create a chemical polymer. The mechanism of polymerization

proposed in Figure 5 starts with the oxidation of dopamine to dopamine quinone which undergoes a Michael-type intramolecular cycloaddition reaction forming leukodopamine-chrome. Its oxidation and subsequent rearrangement form 5,6-dihydroxyindole (DHI). In a covalent pathway two or three monomers of DHI are connected by covalent bonds. In the physical self-assembly (pathways b) several DHI units physically interact with each other by π-π stacking [21].

In contrast to this model, a recent study has reported limited degree of DHI oligomerization. Okuda *et al.* assuming the chemical disorder model of DHI-melanine, solved an equation based on the ratio of two DHI-melanine degradation products, pyrrole-2,3,5-tricarboxylic acid (PTCA) and pyrrole-2,3-dicarboxylic acid (PDCA), showing that the degree of oligomerization is limited up to eight units of DHI oligomers coexisting as tetramers and pentamers[22]. Other studies propose in the same way as Okuda et al. a covalent polymerization model where PDA is mostly constituted by tetramer units[23] [24].

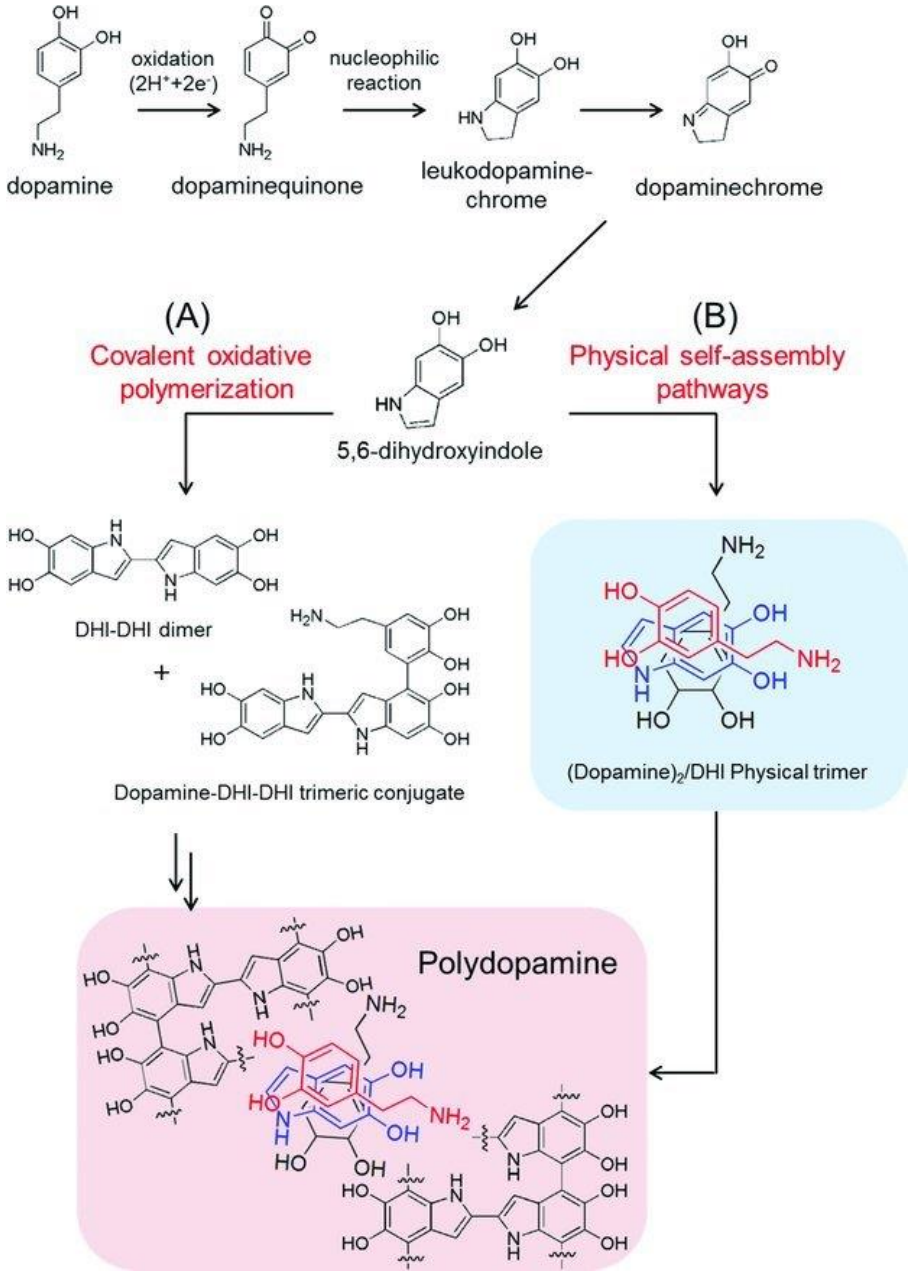

Figure 5:Polydopamine synthesis occurs via two pathways: A) a pathway of covalent bond forming oxidative polymerization and B) a newly proposed pathway of physical self-assembly of dopamine and DHI[21].

Liebscher *et al.*[24]demonstrated that PDA cannot be only a physical polymer but consists of a mixture of different oligomers. The chain contains indole units with different degrees of (un)saturation as well as open chain dopamine units.

Dreyer and co-workers proposed that PDA consist of a supramolecular aggregate composed mainly of 5,6-dihydroxyindoline and dopaminochrome. The bonds between units are believed to be a combination of charge transfer, π-π stacking and hydrogen bonds[25].Hong, Seonki, et al describe a physical trimer $(dopamine)_2$ / DHI[21].

Della Vecchia *et al*. presented that polydopamine consists of three main building blocks, uncyclized catecholamine/quinones, cyclized DHI units and pyrrolecarboxylic acid

moieties. It has been pointed that the Tris buffer used is incorporated in the polymerization [26].

Moreover, the conditions of polymerization have a major impact on the potential mechanism of the dopamine polymerization. Some of these parameters will be mentioned below.

1.7 The coating of polydopamine

The first PDA coating method was developed by Lee *et al.*, where dopamine hydrochloride was dissolved in a 10 mM tris(hydroxymethyl)aminomethane (Tris) buffer solution in order to attain a dopamine concentration of 2mg/mL at pH=8.5[20]. Tris buffer is incorporated into the polymer (Figure 6) and particularly during the oxidation of dopamine at low concentration[26]. Moreover, the incorporation of Tris to the polymer has an impact on the thickness of the film coating[27].

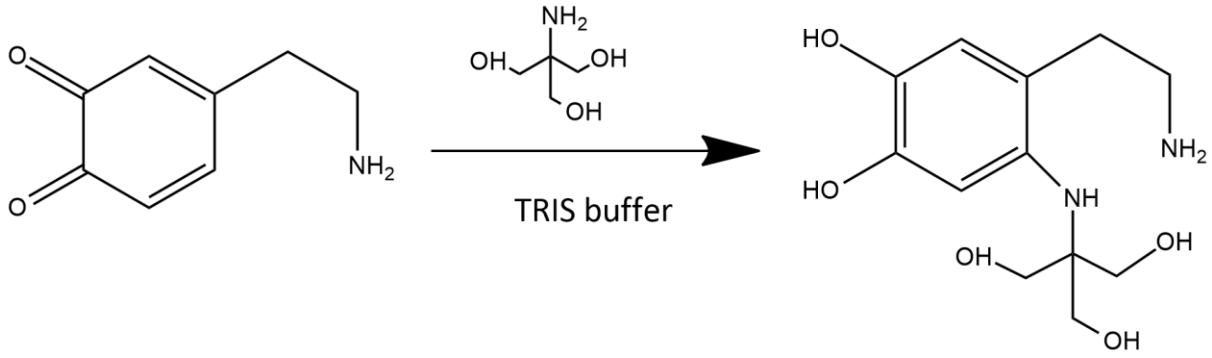

Figure 6: Tris buffer incorporation into dopamine-quinone[28].

Other buffer compounds such as phosphates and bicarbonates are not incorporated in the polymer. Phosphate buffers favor the aggregation of DHI units giving rise to large size PDA particles. At a pH of 8.5 the dopamine is positively charged on the uncyclized side chains and may interact electrostatically with the negatively charged buffer. Therefore, the electrostatic interactions serve as the primer to direct further stacking and charge-transfer interactions between the aromatic moieties. On the other hand, bicarbonate buffers at pH 8.5 are mainly present as monoanion and therefore the effect described above is weaker than with the dianion form of phosphate. Another interesting point is the higher ionic strength in phosphate buffer than Tris and bicarbonate. This phenomenon promotes aggregation when oligomers become hydrophobic[29]. To control PDA particle size ammonia or sodium hydroxide can be employed[30–32].

It has been shown that the polymerization of dopamine in alkaline solution in the presence of O_2 introduced via exogenous ways lead to faster deposition on the support with a smoother morphology than polymerization with only O_2 present in ambient air[33].The kinetics of the polymerization reaction is thus pH dependent. Using weak oxidants like oxygen result in a slow polymerization under neutral conditions; the polymerization rate increases with the pH between pH 8.5-10. To obtain a faster polymerization, ozone and sodium periodate can be used[19].V.Ball *et al.* have studied the kinetic deposition of dopamine[34]. Tris buffer was used and the oxidant was endogenous oxygen. They have found that the deposition at pH 6 was very

slow. They observed a significant increase in film thickness between pH 8.5 and 10.2 as well as with higher concentrations of dopamine. The roughness of the film increased also with dopamine concentration.

In another study conducted by Alfieri *et al.* [35] it has been shown that using a 1mM of dopamine did not lead to detectable film deposition neither with carbonate buffer, Tris nor phosphate. Even with the addition of 1 mM sodium periodate which should induce the fast formation of o-quinone no deposition of dopamine was detected with UV-Visible spectrophotometry. However, when hexamethylenediamine (HMDA), or other amines were added to 1 mM dopamine solution at pH=9, variable levels of coating formation were observed. Long aliphatic chain and two amine groups helped the deposition of polydopamine[19,35]. The incorporation of multiamine compound into the polymerization of PDA on the surface influences the surface charge. The diamine was incorporated into the coating by Michael addition and Schiff base reaction[19]. The incorporation of long and flexible aliphatic chains into the PDA via amine groups would:

- provide hydrophobic component, which is critical for underwater adhesion
- inhibit intramolecular cyclization by occupying specific position or via Schiff-base formation
- inhibit the formation of aggregate which is critical for adhesion[35]

The PDA film formation counts two phases: film deposition and film growth[34]. It has been shown on mica that the adsorption and coating of PDA can be explained by a Wolmer-Weber growth model. First PDA molecules adsorb on the mica surface and serve as the seeding materials, then other PDA particles adsorb around the seeding material to form island-like PDA particles, after other available PDA particles deposit in the gaps between the island-like particles or on the surface of the native particles[36].

To prove that the film formation properties are specifically associated with early intermediates in dopamine autoxidation, the support was introduced at different times after the oxidation has started. The formation of a film is most efficient in the early hours[35].

The polymerization mechanism has an impact on adhesion strength to the surface. In the next section some examples of PDA interaction with several materials are presented.

1.8 Polydopamine interactions with different materials

A strong adhesion is observed in the presence of amine group and catechol. A study was performed to prove it. Three groups were compared: one group with both catechol and amine, another one with catechol removed while maintaining amine, and a group without amine but with catechol. The results showed weak adhesion when one compound was missing, suggesting that a combination of them and the proximity in space of catechol and amine groups are important to initiate strong adhesion[37].

The adhesive property of dopamine related to its capacity to displace water molecules from the surface of surface supports[1838].The variability of the adhesion comes from the

capacity of dopamine to form covalent, hydrogen, π-π interaction and coordination bonds with different materials.

For instance, the adhesion of dopamine on TiO_2 is in part covalent(40%) and in part ionic(60%)[39].The strength of the bond has been measured via atomic force microscopy in contact mode[20]. The strength is due to a ligand-to-metal charge transfer complex between the Ti^{4+} at the surface and the oxygens in the catechol group[40,41].The effect of pH has been studied. At pH < 5.5, dopamine forms two hydrogen bonds with the O of the surface. At pH >8 the hydroxyl groups are partially dissociated, and the O atoms form two coordination bonds with the Ti^{4+} at the surface. At an intermediate pH, there is a combination of one hydrogen bond and one coordination bond[41].Catechol adhesion to wet SiO_2 surfaces occurs by bidentate hydrogen bonding between catechol and SiO_2[38,42]. Finally, the adsorption of catechol on boehmite has been studied[43]. A binuclear complex between catechol group and aluminum ion is possible but only at the surface edge therefore only a small fraction of the surface is concerned.

As regards PDA complexation of metal ions, it is known that PDA can absorb multivalent cations via semiquinone, quinone-imine or carboxylic acid groups[28].PDA can bind metal ions like Au^{3+}, Mn^{2+},Ni^{2+} ,Fe^{3+}, Pt^{4+}, Pd^{2+},Cu^{2+} [44] or Ru^{3+} [45] . The pH has an impact on the bond. For example Fe^{3+} forms a mono-complex with polydopamine under pH 4, a bis-complex between pH 4 and pH 7.5 and a Tris-complex above pH 7.5. [46] In the case of Cu^{2+} below pH 5, Cu^{2+} ions form a complex with carboxyl groups and bidentate nitrogen-carboxyl groups. At pH 7, binding of Cu^{2+} ions occurs at phenolic hydroxyl groups and, at pH above 7, binding of Cu^{2+} ions can be with either three or four nitrogen ligands[47].

2 Objectives and strategy

As reported before, heterogeneous catalysts including ruthenium for the oxidative cleavage of OA into AA and PA is poorly documented. Therefore, the main objective of this work is to synthesize a ruthenium-based heterogenous catalyst for the oxidative cleavage of OA. This catalyst must be recyclable and achieve high conversion and selectivity towards PA and AA.

To reach this objective the following sub-objectives are set:

- Optimization of conditions required for dopamine polymerization on alumina
- Synthesis of Ru-based catalysts via functionalization of alumina with polydopamine
- Evaluation of the synthesized catalysts in the oxidative cleavage of oleic acid

- **Optimization of conditions required for dopamine polymerization on alumina**

In order to gain a better knowledge about PDA deposition on alumina, two supports were selected:α-Al_2O_3 and γ-Al_2O_3.To understand the deposition of polydopamine on alumina, the possibility that the PDA could be partly in the pores and partly on the surface of the support has been eliminated by choosing the non-porous α-Al_2O_3[48].In addition, the incertitude on whether the ruthenium will diffuse in the pores (without knowing whether PDA will be

present therein or not) is avoided, as for the question on the ability on the ability that oleic acid has to go in the pores or not. However, due to the very small specific area of α-Al_2O_3 the amount of PDA required to cover the totality of the surface was too small. To overcome this problem, another alumina with a larger specific surface area but still no porosity was selected; γ-Al_2O_3.The physico-chemical and morphological properties of both supports were determined by: Nitrogen physisorption, thermogravimetric analysis (TGA), FTIR spectroscopy, X-ray photoelectron spectroscopy (XPS) and X-ray diffractometer (XRD). To understand how the dopamine deposits on α-Al_2O_3 and γ-Al_2O_3, several conditions are going to be tested. The impact of the presence of oxygen and the pH will be examined on the deposition of PDA. The optimal pH for a rapid deposition and polymerization of dopamine is between 8.5 and 10[19]. The pH will be then adjusted by the addition of Tris buffer. The decomposition of HMTA in water release NH_3 which is expected to help the polymerization and therefore the Tris buffer will be replaced by HMTA[49]. The deposition of PDA on alumina is expected to be achieved by one homogeneous monolayer covering the surface of the support. It is currently accepted that Tris incorporates via its primary amine groups during the polymerization of PDA[28] which would lead to a thicker film. HMTA does not contain primary amine so it is expected that it will not be incorporated during the polymerization. By doing so, it is expected that the best conditions of the polymerization of dopamine will be found. The term “alumina compound” will now refer to the alumina on which PDA has been deposited.

Like said before, the following protocol has been followed to see the influence of the oxygen, pH and the replacement of tris buffer by HMTA. The denomination used for each solid is reported in the following diagram (Figure 7). The same denomination is used also used for γ-Al_2O_3. The following characterization techniques will be performed: Nitrogen physisorption will be used to known the specific surface area, thermogravimetric analysis (TGA) will give the amount of PDA on the support, FTIR spectroscopy serves to identify the characteristic peaks of PDA deposited on the support, X-ray photoelectron spectroscopy (XPS) serves to determine the presence of PDA on the surface and X-ray diffractometer (XRD) is performed to ensure that the presence of PDA does not affect the integrity of the support.

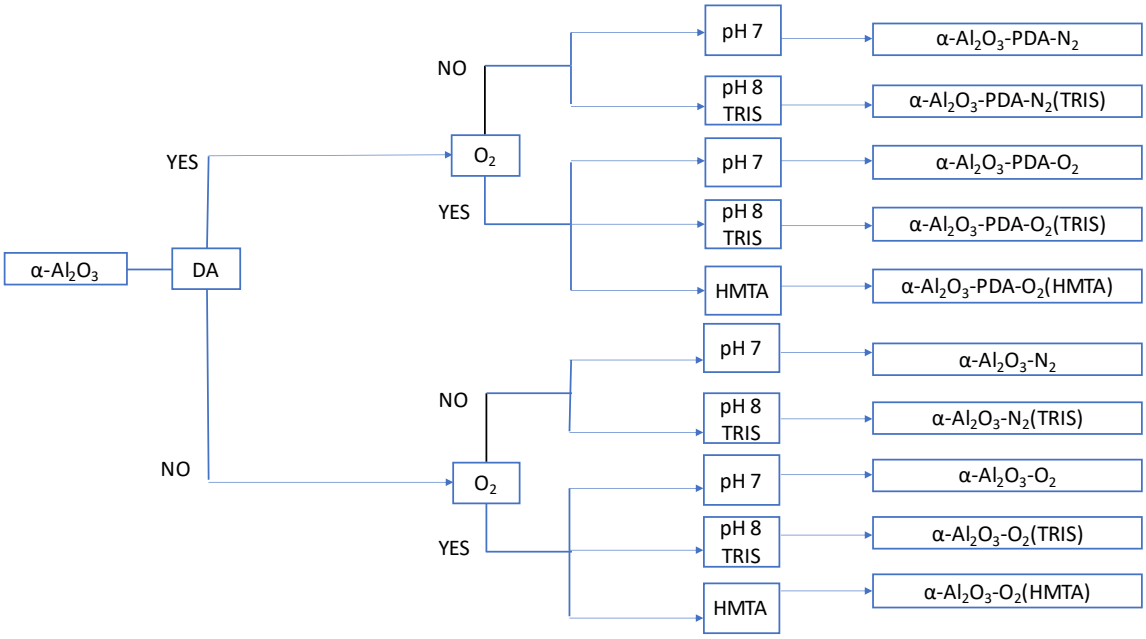

Figure 7: Illustration of the conditions applied to α-Al_2O_3 and their final denomination.

- **Impregnation of Ru on alumina compounds and evaluation of the performance of the synthesized composite in the oxidative cleavage of OA including recycling tests and hot filtration tests.**

The impregnation of ruthenium using $RuCl_3$ is achieved through wet impregnation on the following eventually modified supports:

-α-Al_2O_3
- α-Al_2O_3-PDA-O_2(Tris)
- α-Al_2O_3-PDA-O_2(HMTA)
- γ-Al_2O_3
- γ-Al_2O_3-PDA-O_2 (Tris)
-γ-Al_2O_3-PDA-O_2 (HMTA)

Then, we are going to analyze by XPS the chemical environment after PDA deposition on alumina and to estimate Ru oxidation state on the catalyst surface. In addition, ICP-AES spectrophotometry will serve to determine the amount of ruthenium effectively deposited on the supports in the different synthesized catalysts also called composites:

-α-Al_2O_3-Ru(2%)
- γ-Al_2O_3- Ru(2%)
- γ-Al_2O_3-PDA-O_2(Tris)- Ru(2%)
-γ-Al_2O_3-PDA-O_2(HMTA)- Ru(2%)

- **Evaluation of the synthesized catalysts in the oxidative cleavage of oleic acid**

Catalytic tests will be performed during 24 hours in order to determine from when the highest conversion with the synthesized catalysts is achieved in the oxidative cleavage of pure oleic acid. Recycling tests will be conducted to verify the stability of the synthesized catalysts

while hot-centrifugation tests will be carried out to verify if the oxidative cleavage is performed on the catalyst's surface or not. This are important information to verify the possibility of reusing the synthesized catalyst.

3 Materials and methods

Heptanoic acid (Internal standard, $C_7H_{14}O_2$, >98% GC),nonanal, (NA, $C_9H_{18}O$, >95 % GC), pelargonic acid (PA, $C_9H_{18}O_2$, >98% GC),azelaic acid (AA, $C_9H_{16}O_4$, >98 % GC), tris(hydroxymethyl)aminomethane (TRIS, $C_4H_{11}NO_3$, >99.0 %) and 3-hydroxytyramine hydrochloride (DA, $C_8H_{11}NO_2$,>98 %) were purchased from TCI Chemicals. Ruthenium (III) chloride hydrate, 99.9%(PGM basis), ($RuCl_3.H_2O$, Ru 38 %) , Aluminum oxide, gamma-phase, 99.97% (metals basis) 3-micron APS powder,S.A.80-120 m^2/g and Aluminum oxide, alpha-phase, 99.9% (metals basis) 20-50 micron APS, S.A. 5-6 m^2/g, Hexamethylenetetramine(ACS,99+%) were obtained from Alfa Aesar. Sodium metaperiodate ($NaIO_4$,>+-99%) was obtained from Sigma-Aldrich. Oleic acid (OA, $C_{18}H_{34}O_2$, >99.9 % GC), Acetonitrile (MeCN, C_2H_3N>99.9 % GC) were purchased from Carl Roth. 9-oxononanoic acid (OXO, $C_9H_{16}O_3$, 95 %) and 9,10-dihydroxystearic acid (diol, $C_{18}H_{36}O_4$, 95 %) were obtained from aber GmbH. Potassium bromide for spectroscopy (≥99%) was purchased from Acros Organics.

3.1 Explanation and hypothesis

The catechol groups can form a complex on alumina surface only if the O-O distance in catechol and OH present at the surface are about the same length which is 2.8 Å[43].The compatible O-O distance that allows covalent bond with PDA is not present on α-Al_2O_3[50]. Therefore, only physical interactions between PDA and α-Al_2O_3 are expected.

Dopamine is expected to have a planar orientation with respect to the support[51]. Following this hypothesis, the section occupied by one dopamine molecule can be calculated as a rectangle area, length*width. Here the length is 8.82 Å which corresponds to (b) in Figure 8 B and the width is 5.85 Å which corresponds to (a) in Figure 8B[52].

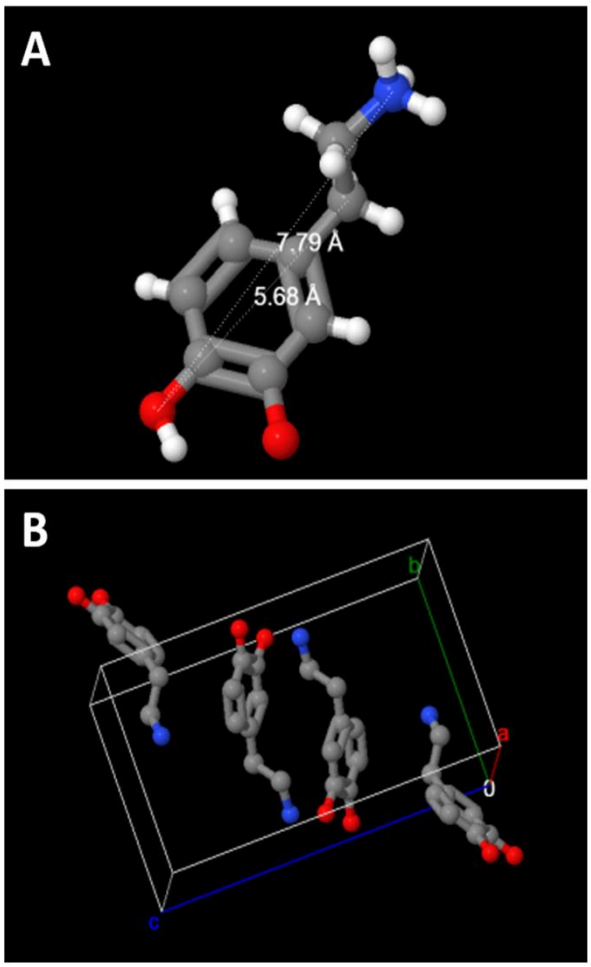

Figure 8: (A) Maximum length of single DA molecule and (B) unit cell length of four DA molecules. a: 5.8528(3) Å, b: 8.8263(5) Å, c: 14.6185 Å, calculated using the Cambridge Crystallographic Data software[51]

Figure 9 shows the interaction between 4 dopamine monomers. Hydrogen bridges will encourage the planar formation of "dopamine sheets" and therefore encourage the dopamine to have a planar orientation with respect to the support.

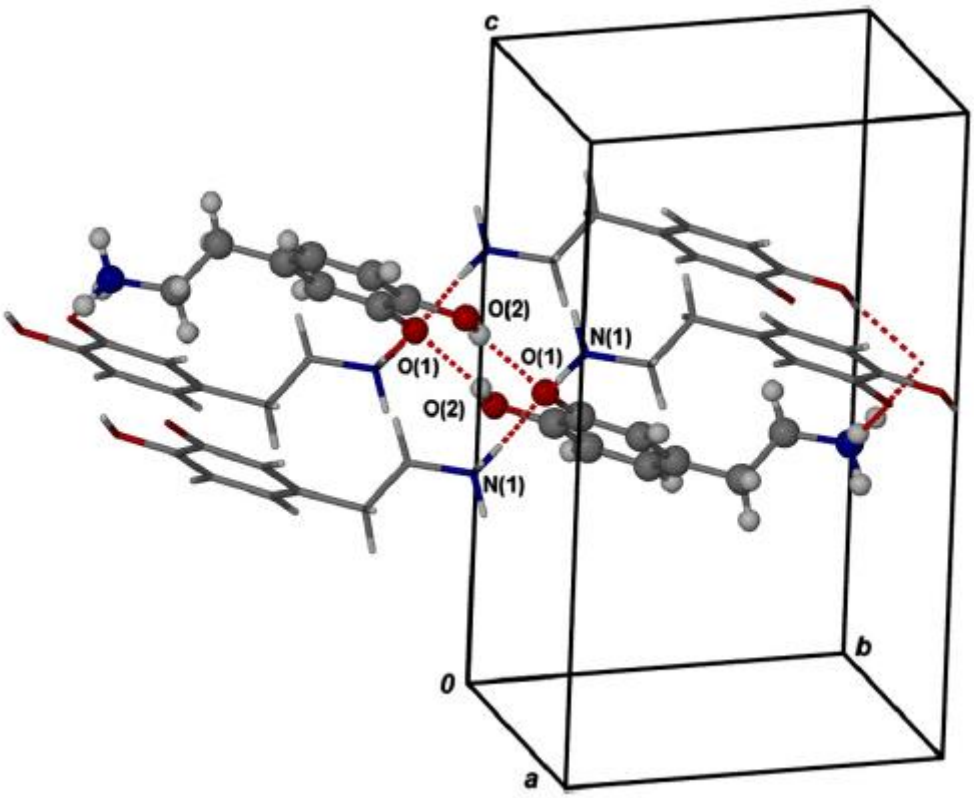

Figure 9: Representation of hydrogen bridges between 4 dopamine monomer[52].

3.2 Calculation of the amount of dopamine required to form a monolayer of PDA on α-Al_2O_3

Under the hypothesis that dopamine will have a planar orientation with respect to the support[51],the surface area occupied by one dopamine molecule therefore can be calculated as rectangle area, length*width. Here the length is 8.82 Å and the width is 5.85 Å[52].

Area occupied on the support by one dopamine molecule:

S=Width x length= 5.8528 x 8.8263 = 51.65 Å² = 5.165 10^{-19} m²

Al_2O_3 S_{bet}= 5.8 $\frac{m^2}{g}$ the surface area developed by 1 g is 5.8 m².

The number of dopamine molecules required to cover the surface of 1 g of α- Al_2O_3:

Number of molecules = $\frac{5.8}{5.16510\text{^}-19}$ =1.2294 10^{19}

Knowing that M_w(dopamine) = 153.17 $\frac{g}{mol}$

For one dopamine molecule

M_w(dopamine) = 153.17 / 6.022 10^{23} = 2.54344 10^{-22} $\frac{g}{molecule\ dopamine}$

Therefore, the mass of dopamine can be calculated as follow to cover 1 g of α-Al_2O_3

Masse (dopamine) = 1.2294 10^{19}x 2.54344 10^{-22}=2.85 10^{-3} g

To cover 4 g of α- Al_2O_3 , 0.0114 g is required.

3.3 Calculation of the amount of dopamine required to form a monolayer on γ-Al_2O_3

γ-Al_2O_3 S_{bet}= 70 $\frac{m^2}{g}$ the surface area developed by 1 g is 70 m².

The number of dopamine molecules required to cover the surface of 1 g of γ-Al_2O_3:

Number of molecules = $\frac{70}{5.16510\text{^}-19}$ =1.3553 10^{20}

Mass of dopamine= 1.3553 10^{20} x 2.54344 10^{-22}=0.03447 g

To cover 4 g of γ- Al_2O_3, 0.13788 g is required.

3.4 Solution 1

The solution 1 is used for the deposition of PDA on α-Al_2O_3. First, 200mL of deionized water was added to a beaker and purged with a N_2 flow in order to eliminate the presence of O_2. Then, 0.014 g of dopamine hydrochloride was dissolved by magnetic stirring. The pH and the O_2 concentration were monitored by pH paper and an OXY-4 mini fiber optic oxygen meter connected to an optical oxygen sensor (PreSens GmbH, Germany) glued on the inner side of a closed reaction vessel equipped with a magnetic stirrer. The dopamine at neutral pH is in its cationic state[53].

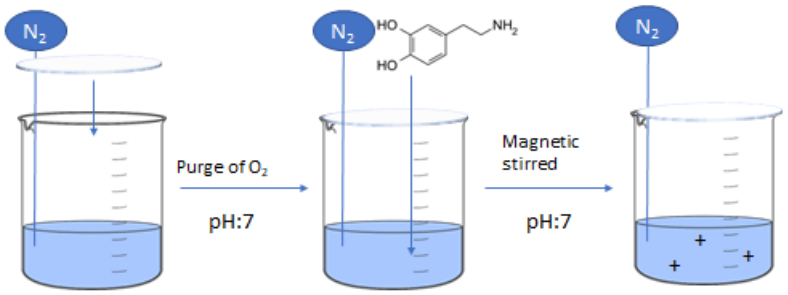

Figure 10: Preparation of the solution 1

3.5 α-Al_2O_3-PDA-N_2

4 g of α-Al_2O_3 was added at the solution 1. The solution was kept under magnetic stirring under nitrogen atmosphere for 1 hour. Then the pH was registered. Finally, the solid was obtained by vacuum filtration (MF-Millipore, pore size = 0.025 µm) and dried in a furnace during 3 hours at 105°C.

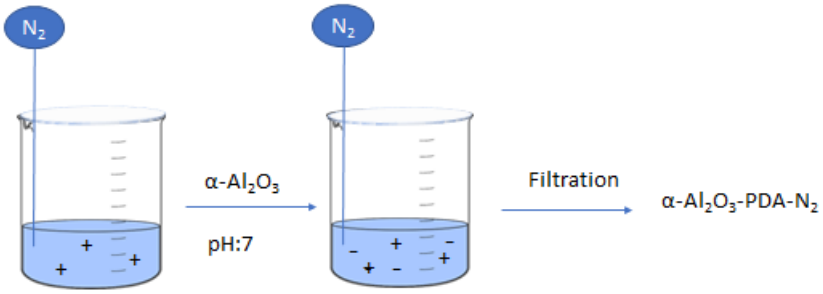

Figure 11: Preparation of the α-Al_2O_3-PDA-N_2

3.6 α-Al_2O_3-PDA-N_2(TRIS)

First,4 g of α-Al_2O_3 was added at the solution 1. Then 0.242 g of Tris (10 mM) was added. The solution was kept under magnetic stirring under nitrogen atmosphere for 1 hour at a pH of 8. Then the pH was registered. Finally, the solid was obtained by vacuum filtration (MF-Millipore, pore size = 0.025 µm) and dried in a furnace during 3 hours at 105°C.

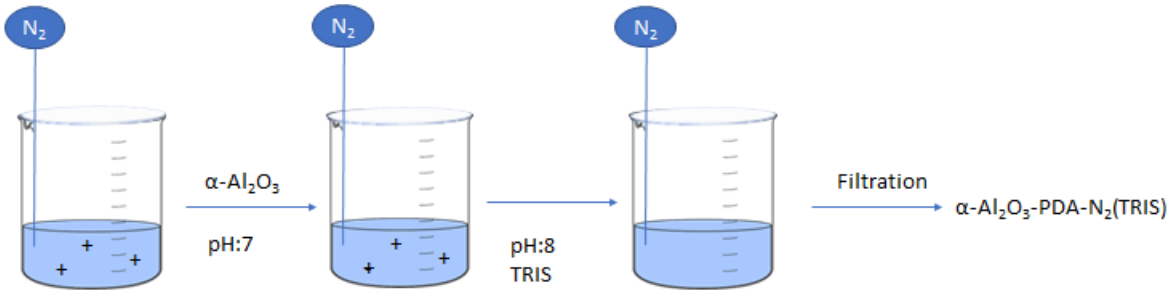

Figure 12:Preparation of the α-Al_2O_3-PDA-N_2(TRIS)

3.7 α-Al_2O_3-PDA-O_2

4 g of α-Al_2O_3 was added at the solution 1. The flow of nitrogen was then replaced by a flow of air. The solution was kept under magnetic stirring for 1 hour at a pH of 7. Afterwards the pH was registered. Finally, the solid was obtained by vacuum filtration (MF-Millipore, pore size = 0.025 µm) and dried in a furnace during 3 hours at 105°C.

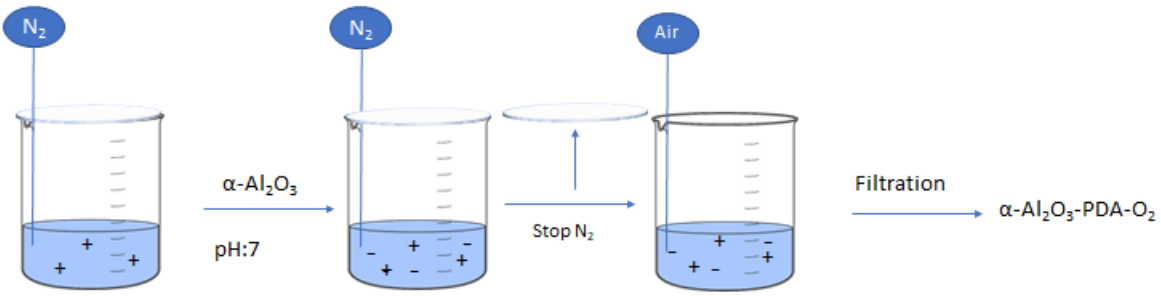

Figure 13: Preparation of the α-Al_2O_3-PDA-O_2

3.8 α-Al_2O_3-PDA-O_2(TRIS)

First, 4 g d' α-Al_2O_3 was added at the solution 1. The flow of nitrogen was then replaced by a flow of air. Afterwards 0.24228 g of Tris (10 mM) was added. The solution was maintained under magnetic stirred for 1 hour at a pH of 8. Then the pH was registered. Finally, the solid was obtained by vacuum filtration (MF-Millipore, pore size = 0.025 µm) and dried in a furnace during 3 hours at 105°C.

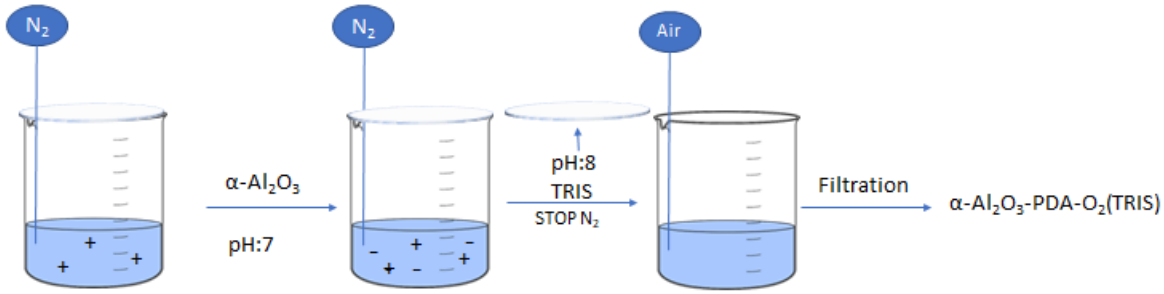

Figure 14: Preparation of the α-Al_2O_3-PDA-O_2(TRIS)

3.9 α-Al_2O_3-PDA-O_2(HMTA)

4 g of α-Al_2O_3 was added at the solution 1. The flow of nitrogen was then replaced by a flow of air. Afterwards 0.28 g of HMTA (10 mM) was added. Thanks to pH paper we checked that the solution is at pH 8. The solution was maintained under magnetic stirred for 1 hour. The pH was registered. Finally, the solid was obtained by vacuum filtration (MF-Millipore, pore size = 0.025 µm) and dried in a furnace during 3 hours at 105°C.

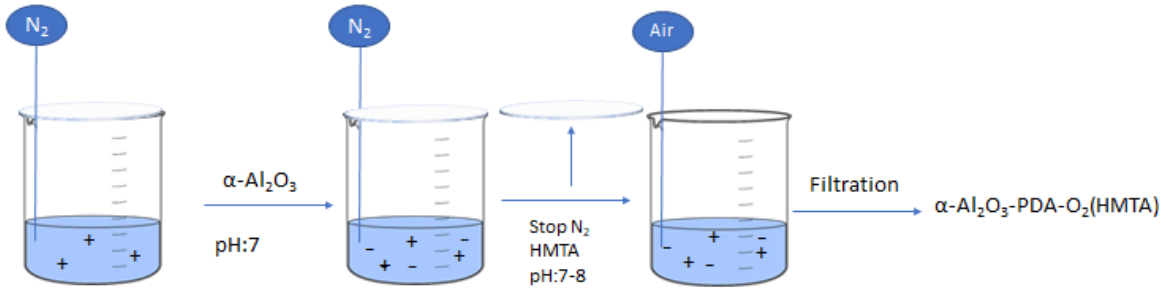

Figure 15: Preparation of α-Al_2O_3-PDA-O_2(HMTA)

3.10 Solution 2

First, 200mL of deionized water was added to a beaker and purged with a N_2 flow in order to eliminate the presence of O_2. Then, 0.138 g of dopamine hydrochloride was dissolved by magnetic stirring. The pH and the O_2 concentration were monitored by pH paper and an OXY-4 mini fiber optic oxygen meter connected to an optical oxygen sensor (PreSens GmbH, Germany) glued on the inner side of a closed reaction vessel equipped with a magnetic stirrer.

3.11 γ-Al_2O_3-PDA-O_2(TRIS)

4 g of γ -Al_2O_3 was added at the solution 2. The flow of nitrogen was replaced by a flow of air. Then 0.242 g of Tris (10 mM) was added. Thanks to pH paper we have checked that the solution was at pH 8. The solution was maintained under magnetic stirred for 1 hour. The pH was registered. Finally, the solid was obtained by vacuum filtration (MF-Millipore, pore size = 0.025 µm) and dried in a furnace during 3 hours at 105°C.

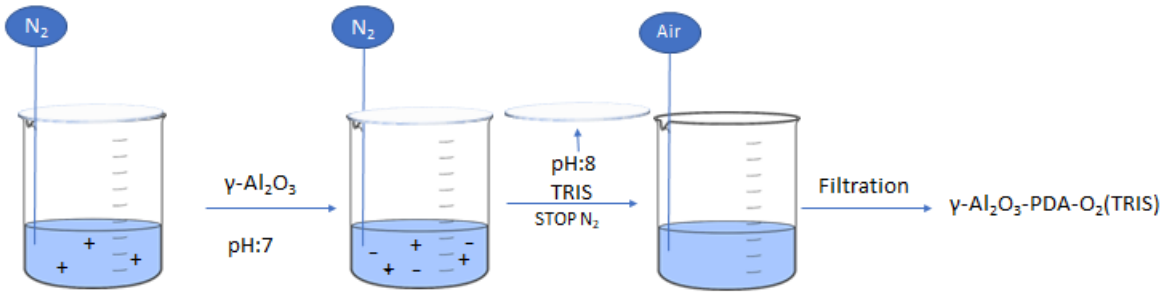

Figure 16: Preparation of γ-Al_2O_3-PDA-O_2(TRIS)

3.12 γ-Al_2O_3-PDA-O_2(HMTA)

First, 4 g of γ -Al_2O_3 was added at the solution 2. The flow of nitrogen was replaced by a flow of air. 0.28 g of HMTA (10 mM) was added. Thanks to pH paper we have checked that the solution was at pH 8. The solution was maintained under magnetic stirred for 1 hour. The pH was registered. Finally, the solid was obtained by vacuum filtration (MF-Millipore, pore size = 0.025 µm) and dried in a furnace during 3 hours at 105°C.

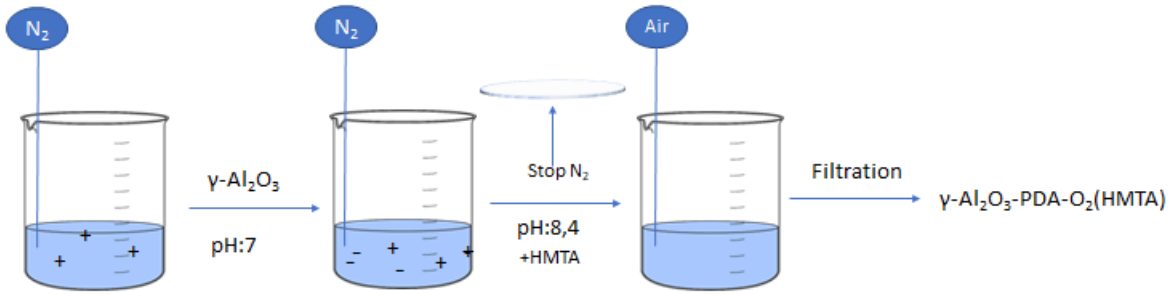

Figure 17:Preparation of γ-Al_2O_3-PDA-O_2(HMTA)

3.13 Impregnation of ruthenium

For solids γ-Al_2O_3-PDA(TRIS), γ-Al_2O_3-PDA(HMDA), α-Al_2O_3-PDA(TRIS) and α-Al_2O_3-PDA(HMDA), 1 g of solid was put into 20 mL of distilled water. The suspension was dispersed by ultrasonic treatments for 15 minutes. Then 10 mL of $RuCl_3.H_2O$ (10mM;0.045g) was added drop by drop in order to obtain a Ru load of 2 wt.% and the mixture was stirred for 24 hours. The separation of the synthesized catalysts denoted as γ-Al_2O_3-PDA(TRIS)-Ru(2%), α-Al_2O_3-PDA(TRIS)-Ru(2%),γ-Al_2O_3-PDA(HMTA)-Ru(2%) and α-Al_2O_3-PDA-(HMTA)-Ru(2%) was

achieved by centrifugation at 14 000 rpm (26 200 g) in a Heraeus MultifugeX1R Centrifuge for 20 minutes. Finally, the catalysts were dried in ambient air at room temperature overnight.

4 Characterization

4.1 Nitrogen physisorption

The textural properties were obtained through N_2 physisorption at -196°C in a Micromeritics Tristar 3000. The specific surface area was calculated thanks to the Brunauer-Emmett-Teller (BET) model using the data in the range of partial pressure {0.05-0.3}. The pore volume and the average pore diameter are calculated with the Barrett-Joyner-Halenda (BJH) method. Samples were weighted (about 200 mg while using a filler rode) before and after degassing for 6 hours with a Micromeritics VacPrep 061 instrument at 150°C and ~10.7 Pa.

4.2 Fourier-transform infrared spectroscopy (FTIR)

25 mg of sample was mixed with 250 mg of KBr. The mixture was pressed as a wafer at 10 T in a Graseby Specac hydraulic press and analyzed with an Equinox 55 FTIR spectrometer (Bruker) in the transmission mode. The outgoing beam was detected by a dielectric DTGS with an iris aperture of 5000 µm. KBr pastille was recorded and used as background. One hundred scans were performed in the range of 4000 to 400 cm^{-1} with a 4 cm^{-1} resolution.

The same instrument equipped with a Platinum ATR cell was used also in the attenuated total reflectance (ATR) mode. One hundred scans were performed in the range of 4000 to 400 cm^{-1} with a resolution of 4cm^{-1}.ATR correction and data processing were performed using the OPUS Software from Bruker.

4.3 X-ray diffractometer (XRD)

The samples were analyzed in a Bruker-D8 Advance diffractometer with a Bragg-Brentano geometry. The X-ray source is a copper anode under 40 kV, 30 mA (Kα=0.154 nm). The detection was achieved with a LynxEye XE-T technology. The angle (2θ) was scanned from 5° to 80 ° at a speed of 6 °/min (5051 steps of 0.015°). Nivea cream was gently applied on the sample-holder to fix the powder which is then deposited homogeneously. The identification of phases was realized by the comparison of the experimental diffractograms and those in the database (ICDD-PDF2-2004) using the EVA software from Bruker.

4.4 X-ray photoelectron spectroscopy (XPS)

Samples were analyzed with a SSX 100/206 photoelectron spectrometer from Surface Science Instruments (USA) equipped with a monochromatized micro focused Al X-ray source (powered at 20 mA and 10 kV). The pressure in the analysis chamber was around 10^{-6} Pa. The angle between the surface and the axis of the analyzer lens was 55°. The analyzed area was approximately 1.4 mm^2 and the pass energy was set at 150 eV. With these above parameters the full width measured at half maximum (FWHM) of the Au $4f_{7/2}$ peak for a clean gold standard sample was about 1.6 eV. The samples powders were pressed in small stainless-steel troughs of 4 mm diameter and placed on a ceramic carousel. A flood gun set at 8 eV and a Ni grid placed above the sample surface are applied for the charge stabilization. The following sequence of the spectra was recorded: survey spectrum, C 1s, O 1s, N 1s, Cl 2p, Ru 3p, Al 2p.

For all the samples, C1s spectrum was double recorded to verify the stability of the charge compensation with time. The aromatic C-(C,H) component of the C 1s peak of carbon has not been set has at 284.8 eV to serve as a reference scale because PDA, HMTA and tris contains carbon. So, Al 2p has been set at 74 eV and serves as a reference scale. Data treatment was performed with the CasaXPS program (Casa Software Ltd, UK). All spectra were decomposed with the least squares fitting routine with a Gaussian/Lorentzian (85/15) product function and after subtraction of a non-linear baseline.

4.5 Thermogravimetric analysis (TGA)

About 20 mg of the solids was introduced into 70 µL Al_2O_3 clean crucibles. A Mettler Toledo TGA/SDTA851e Thermogravimetric Analyzer is used. All analyses are performed under a nitrogen atmosphere at a flow rate of 40 mL/min from 50°C to 900°C with a heating ramp at 10°C/min.

4.6 Inductively coupled plasma-atomic emission spectroscopy (ICP-AES)

Ruthenium load on each carbon catalyst was measured by inductively coupled plasma - atomic emission spectrometry (ICP-AES) in an ICP 6500 Thermo Scientific Instrument. For this matter, about 100 mg of each sample was placed in a vitreous carbon crucible and calcined overnight at 500 °C in an oven to remove the organic matter. Then, 50 to 100 mg of the calcined sample was mixed with 2 g of sodium peroxide (Na_2O_2) along with 1 g of sodium hydroxide tablet (NaOH) and transferred to another vitreous carbon crucible. This solid mixture was molten under the flame of a Bunsen burner and after cooling, the crucible was immersed in 100 mL of HCl 11 % (v/v) solution to dissolve all Ru along the carbonaceous matrix. Finally, the crucible was rinsed with distilled water and the obtained solution was diluted to 1000 mL prior analysis.

4.7 Catalytic test

In a closed 20 mL vessel 438 mg of $NaIO_4$ was dissolved in 8mL of H_2O with magnetic agitation at room temperature. After 4 mL of acetonitrile, 2 mL of ethyl acetate, 196 µL of oleic acid and 81.5 µL of heptanoic acid (Internal standard) were added. An aliquot of 0.2 mL from the organic phase was extracted and diluted in 1.3 mL of ethyl acetate. Afterwards 100 mg of the catalyst was added. The reaction was monitored by taking aliquots of 0.2 mL from the organic phase after 2, 4, 6 and 24 hours.

Every extraction was done with a 1mL Injekt®-F Luer Solo syringe from B Braun and filtrated (MF-Millipore, pore size= 0.25µm). All samples were analyzed in a Varian 3800 Gas Chromatograph (GC) equipped with a Flame Ionization Detector (FID). In this study, a Stabilwax-DA Restek column, formed by a crossbond acid-deactivated Carbowax polyethylene glycol as stationary phase, was employed in order to inject directly the samples without performing any derivatization process. The GC has a split ratio of 35:1 with a pressure of 10 psi. The FID temperature was set at 300°C and the injector at 285°C. The oven was first hold at 100 °C for 2 minutes and then it was increased until 240°C (8°C/min).

Conversions were calculated with the following equation:

$$C = \frac{n_{OA\ t=0} - n_{OA\ t=t*}}{n_{OA\ t=0}}$$

where C is the conversion, $n_{OA\ t=0}$ is the initial quantity in mole of OA before adding the catalyst and $n_{OA\ t=t*}$ is the quantity of OA at a given time t*.

Selectivities were calculated with the following equation:

$$S = \frac{n_{p,t=t*}}{n_{OA\ t=0} - n_{OA\ t=t*}} = \frac{mol\ of\ desired\ product}{mol\ of\ converted\ OA}$$

where $n_{p,t=t*}$ is the number of moles of product produced at a given time t*. The number of moles is calculated based on the calibration curves (Appendices). AA is slightly soluble in the aqueous phase; the concentration is therefore corrected by the partition coefficient K_{AA} which is calculated via:

$$K_{AA} = \frac{C_{AA_{aq}}}{C_{AA_{org}}} = 0.175\ \pm 0.003$$

where $C_{AA\ aq}$ is the concentration of AA in water and $C_{AA\ org}$ is the concentration of AA in AcOEt. K_{AA} was calculated by Sebastian Gamez, using the data he obtained during his PhD thesis. The total quantity of products is then the sum of the amount of AA dissolved in each phase.

$$n_p(tot)\ =\ n_p(aq)\ +\ n_p(org)$$

4.8 Recycling tests

After 24 hours of catalytic test, the catalyst was separated from the solution by centrifugation. The centrifugation was performed in a Heraeus Multifuge X 1R Centrifuge from Thermo Scientific at 14 000 rpm (26200 g), 25 °C and during 20 minutes. After removing the solution, the solid was dried under ambient temperature in ambient air during the night. Then the catalyst was re-injected in a fresh reaction mixture to perform the oxidative cleavage of oleic acid with the same procedure as mentioned above. This procedure was repeated 5 times to check the possibility to re-use the catalysts. Conversion and selectivity were calculated after each recycling test.

4.9 Hot centrifugation tests

In these tests, once the conversion in a test described above was approximately 50 %, the catalyst was removed from the reaction medium by centrifugation. The centrifugation was performed in a Heraeus Multifuge X 1R Centrifuge from Thermo Scientific at 14 000 rpm (26200 g), 25 °C and for 20 minutes. Then, the reaction continued to be monitored (without the solid catalyst) by injecting samples of the organic layer in the chromatograph. This test was performed to verify whether the oxidative cleavage kept ongoing after the removal of the solid catalyst. An increase in conversion after the catalyst removal would suggest that the active sites (ruthenium species) are in the liquid phase instead of on the composite surface.

5 Results and discussion

5.1 Validation of best conditions for the deposition of PDA

FTIR and XPS spectroscopy were performed to verify the presence of PDA on α-Al_2O_3 and γ-Al_2O_3. For α-Al_2O_3 a broad band is displayed at 3443 cm^{-1} which may correspond to hydrogen-bonded surface hydroxyl groups. The broad band in the range of 600-800 cm^{-1} and the peak at 463 cm^{-1} correspond to Al-O stretching vibration. The peak at 1639 corresponds to H_2O. These results are in accordance with previous research [54].For γ-Al_2O_3 the 2 broad bands at 3393 cm^{-1} may be attributed to O-H stretching vibration of H_2O. The 3111 cm^{-1} peak may correspond to stretching vibration in AlOOH. The peak at 1105 cm^{-1} corresponds to plane-bending scissoring vibration of OH in AlOOH[55](Figure 18).

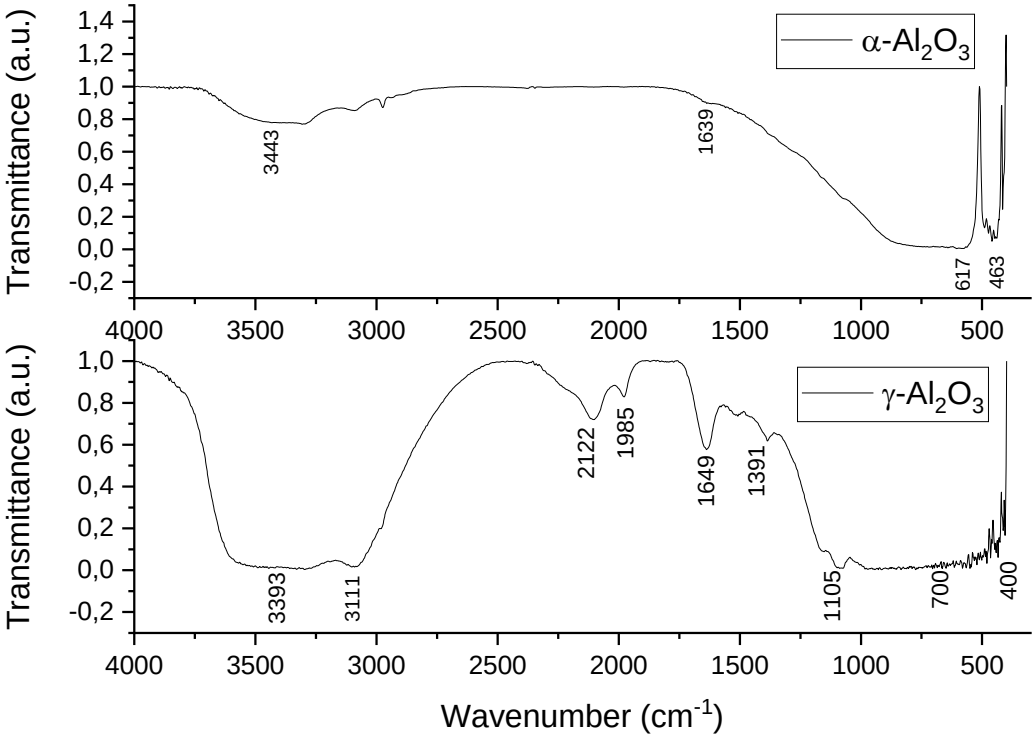

Figure 18:FTIR spectra of α-Al_2O_3 and γ-Al_2O_3.

After PDA deposition on γ-Al_2O_3, a peak appears at 1508 cm^{-1} which can be due to N-H bending (Figure 19a), the 2 peaks at 1539 cm^{-1} and 1472 cm^{-1} could be attributed to N-H stretching and scissoring because of the indole or indoline structure of PDA, 1389 cm^{-1} can be associated to C-H bending and 1350 cm^{-1} to C-N stretching (Figure 19b). The amount of dopamine added to α-Al_2O_3 was too small to be seen in FTIR (Figure 20).

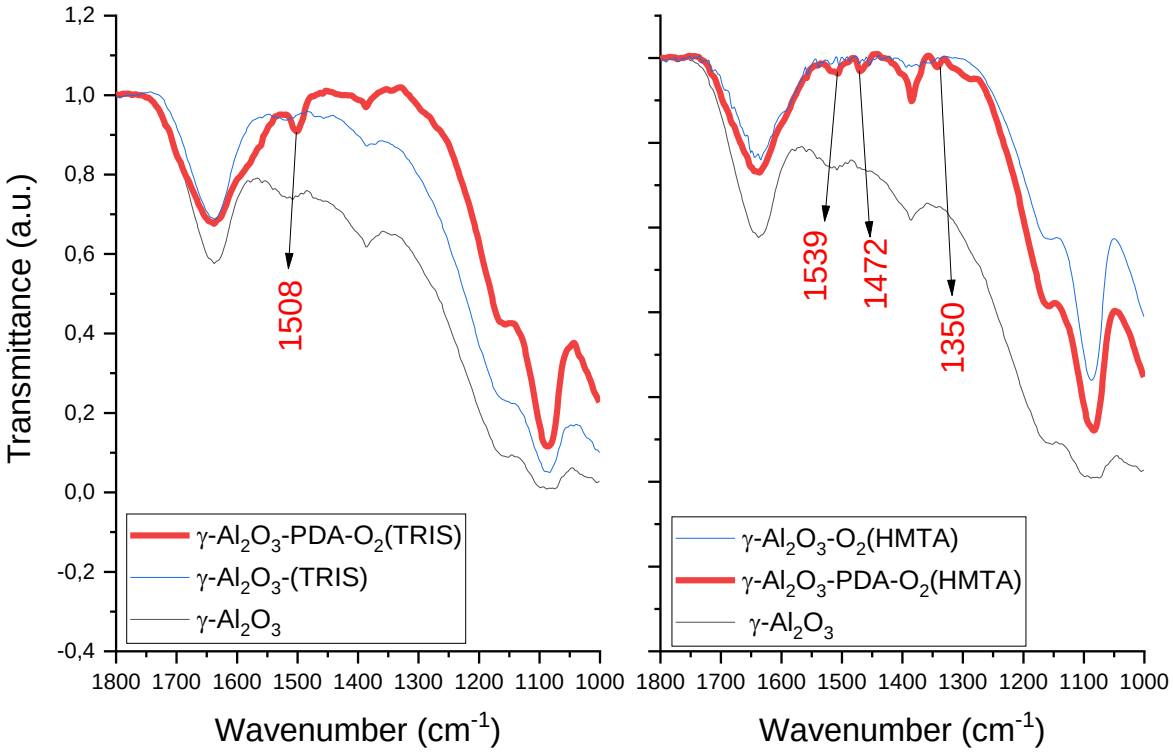

Figure 19: FTIR spectra of (a) γ-Al_2O_3, γ-Al_2O_3-O_2(TRIS) and γ-Al_2O_3-PDA-O_2(TRIS) ,(b) γ-Al_2O_3, γ-Al_2O_3-O_2(HMTA) and γ-Al_2O_3-PDA-O_2(HMTA)

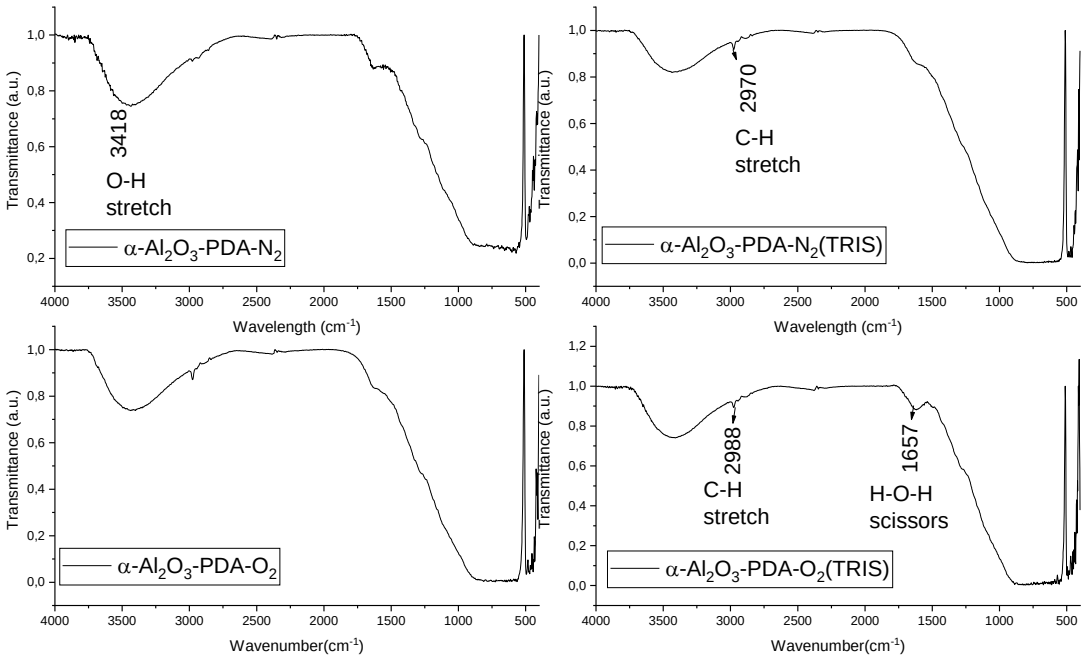

Figure 20: FTIR spectra of (a) α-Al_2O_3-PDA-N_2, (b) α-Al_2O_3-PDA-N_2(TRIS), (c) α-Al_2O_3-PDA-O_2 and (d) α-Al_2O_3-PDA-O_2(TRIS).

The deposition of polydopamine was successful for α-Al_2O_3-PDA-O_2(TRIS), α-Al_2O_3-PDA-O_2(HMTA) , γ-Al_2O_3-PDA-O_2(TRIS) because nitrogen is detected in their survey spectra XPS and also in the survey (Table1). The high-resolution N1s spectrum shows a well-defined peak for α-Al_2O_3-PDA-O_2(TRIS) (Figure 21d). The high-resolution N1s spectrum of α-Al_2O_3-N_2(Figure 21e) and α-Al_2O_3-O_2(Figure 21g) present a small peak which is due probably due to skin contamination because the certificate of Analysis (ICP) provided by Alpha does not reveal the presence of nitrogen and the solid was not put in presence of any nitrogen compounds (other than the flux of N_2 for α-Al_2O_3-N_2). For α-Al_2O_3-PDA-N_2(Tris) (Figure21b), α-Al_2O_3-N_2(TRIS) (Figure 21f) and for α-Al_2O_3-O_2(TRIS) the peak detected is due to the deposition of TRIS on the support. In appendices (Figure 32), the deposition of HMTA is also observed. In conclusion the deposition of PDA requires oxygen and alkaline conditions. In addition, the nitrogen comes from PDA and either TRIS or HMTA which are adsorbed on the support.

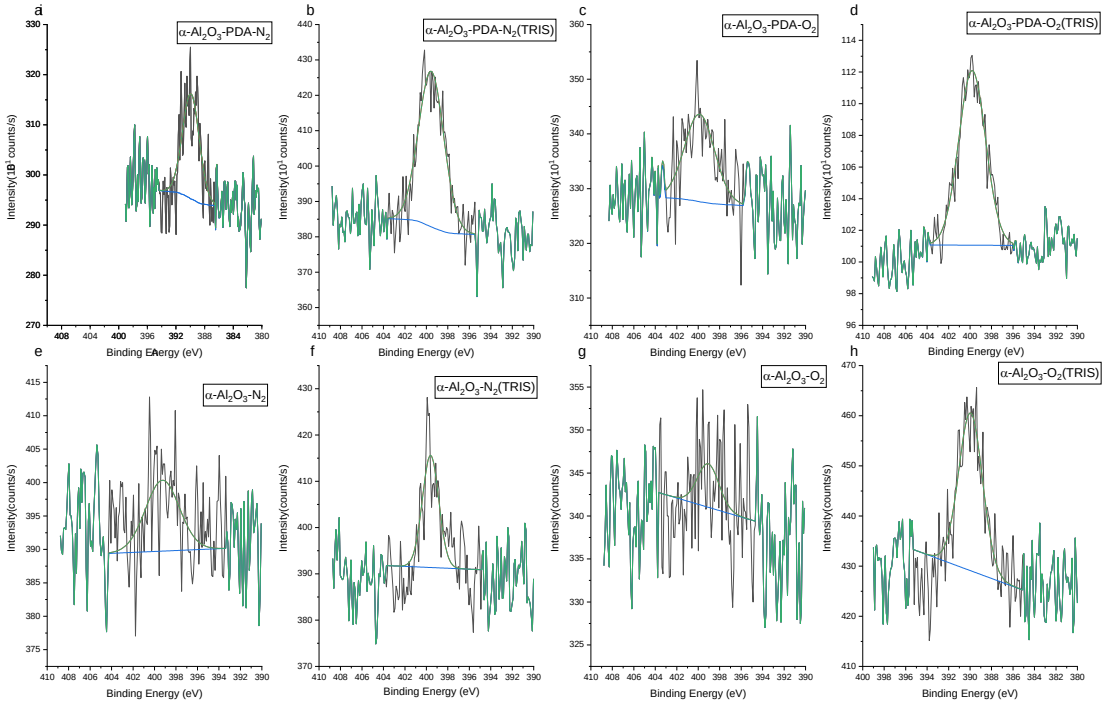

Figure 21: High resolution N1s spectrum of(a) α-Al_2O_3-PDA-N_2, (b) α-Al_2O_3-PDA-N_2(TRIS), (c) α-Al_2O_3-PDA-O_2, (d) α-Al_2O_3-PDA-O_2(TRIS), (e) α-Al_2O_3-N_2, (f) α-Al_2O_3-N_2(TRIS), (g) α-Al_2O_3-O_2 and (h) α-Al_2O_3-O_2-(TRIS).

The deconvolution of N1s spectra for γ-Al_2O_3-PDA-O_2(TRIS)-Ru (Figure 22a) and of γ-Al_2O_3-PDA-O_2(HMTA)-Ru (Figure 22b) shows the presence of primary amine (R-NH_2) which can be the consequence of an incomplete cyclization. In the case of γ-Al_2O_3-PDA-O_2(TRIS)-Ru this may be due to the incorporation of tris during polymerization (Figure 6). The species R-NH-R and R=N-R are corresponding to secondary amines and imine on the indole ring of polydopamine.

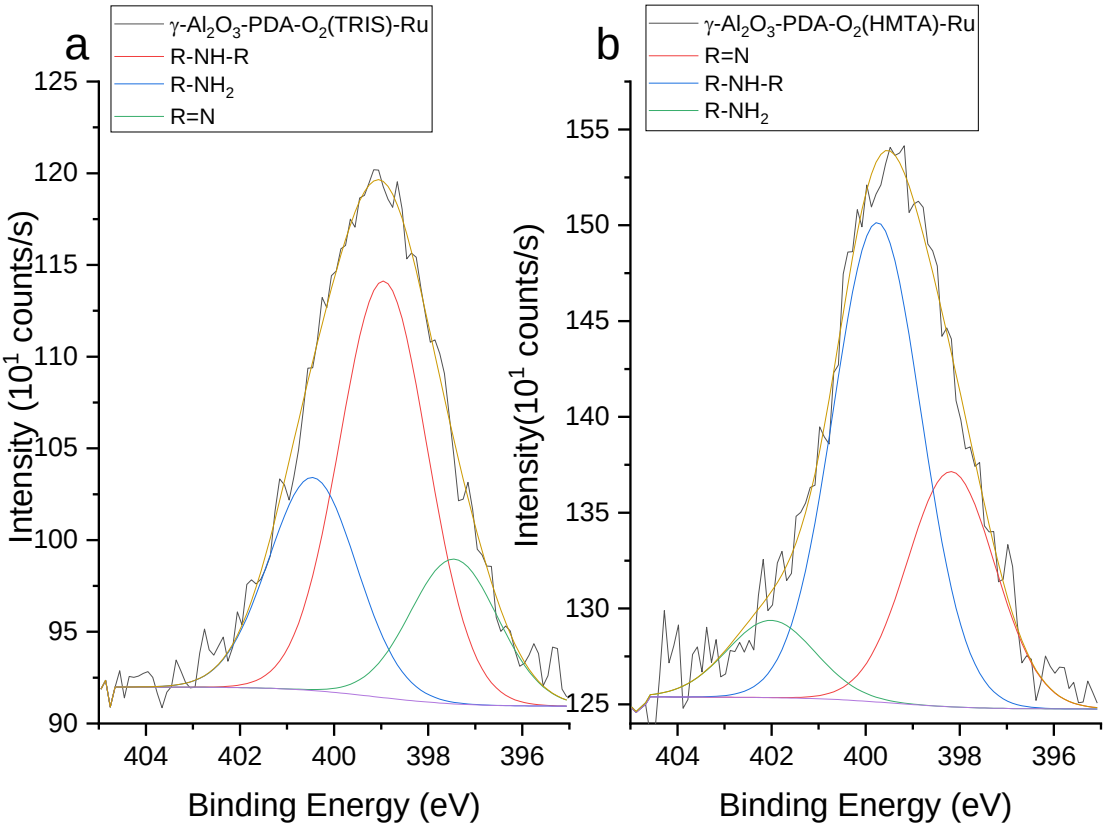

Figure 22: Deconvoluted N1s spectra of (a) γ-Al_2O_3-PDA-O_2(TRIS)-Ru and (b) γ-Al_2O_3-PDA-O_2(HMTA)-Ru.

Table 1: Superficial chemical composition (from XPS) of α-Al_2O_3, α-Al_2O_3-PDA-N_2, α-Al_2O_3-PDA-N_2(TRIS), α-Al_2O_3-PDA-O_2, α-Al_2O_3-PDA-O_2(TRIS), α-Al_2O_3-N_2, α-Al_2O_3-N_2(TRIS), α-Al_2O_3-O_2 ,α-Al_2O_3-O_2-(TRIS) γ-Al_2O_3, , γ-Al_2O_3-PDA-O_2(TRIS), γ-Al_2O_3-O_2(TRIS) , γ-Al_2O_3-PDA-O_2(HMTA) and γ-Al_2O_3-O_2(HMTA).

Sample	O1s	C1s	Al2p	N1s
α-Al_2O_3	62.5	8.9	28.5	-
α-Al_2O_3-PDA-N_2	68.4	12,1	19,5	-
α-Al_2O_3-N_2	65.8	8.8	25.3	-
α-Al_2O_3-PDA-N_2(TRIS)	65.9	12.6	21.5	-
α-Al_2O_3-N_2(TRIS)	68.8	9.6	21.5	-
α-Al_2O_3-PDA-O_2	56.5	15.7	27.7	-
α-Al_2O_3-O_2	69.8	10.7	19.4	-
α-Al_2O_3-PDA-O_2(TRIS)	57.9	16.4	24.78	0.9
α-Al_2O_3-O_2(TRIS)	68.1	10.8	21	-
α-Al_2O_3-PDA-O_2(HMTA)	52.7	13.2	33.84	0.3
α-Al_2O_3-O_2(HMTA)	66.5	7.2	26.33	-
γ-Al_2O_3	55.9	13	30.97	-
γ-Al_2O_3-PDA-O_2(TRIS)	56.4	9.5	33.7	0.3
γ-Al_2O_3-O_2(TRIS)	58.6	7.3	33.8	0.3
γ-Al_2O_3-PDA-O_2(HMTA)	57	7.6	35.3	-
γ-Al_2O_3-O_2(HMTA)	66.5	7.2	26.3	-

5.2 Evaluation of the impact of the deposition of PDA on the support

Textural properties of α-Al_2O_3, α-Al_2O_3-PDA-O_2(TRIS), γ-Al_2O_3 and γ-Al_2O_3-PDA-O_2(TRIS) using the N_2 physisorption isotherms (Figure 23) were calculated (Table 2). The four isotherms present a type II shape with a weak hysteresis starting after above P/P_0=0.9 but hystereses are considered too weak to consider a type IV isotherm.Type II isotherm are typical of macroporous or non-porous solids[56].The particles are non-porous, the porosity arises from macropore between particles. There are no significant differences when PDA is deposed on α-Al_2O_3. However, when PDA is deposited on γ-Al_2O_3 the specific surface area is decreasing because PDA is recovering in one layer every particle and therefore fill the defect present at the surface. The pore volume and the pore diameter are increasing because the particles are bigger due to the monolayer of PDA and therefore the space between the particles are bigger.

Table 2: Textural properties of α-Al_2O_3, α-Al_2O_3-PDA-O_2(TRIS), γ-Al_2O_3 and γ-Al_2O_3-PDA-O_2(TRIS)

Sample	Pore diameter (nm)	Specific surface area (m^2/g)	Pore volume ($cm^3/gSTP$)
α-Al_2O_3	27	6	0.021
α-Al_2O_3-N_2	25	7	0.024
α-Al_2O_3-PDA-N_2	21	8	0.025
α-Al_2O_3-N_2(TRIS)	24	7	0.025
α-Al_2O_3-PDA-N_2(TRIS)	25	8	0.028
α-Al_2O_3-O_2	36	7	0.02
α-Al_2O_3-PDA-O_2	25	7	0.029
α-Al_2O_3-O_2(TRIS)	22	8	0.029
α-Al_2O_3-PDA-O_2(TRIS)	28	8	0.029
α-Al_2O_3-O_2(HMTA)	16	6	0.015
α-Al_2O_3-PDA-O_2(HMTA)	28	8	0.031
γ-Al_2O_3	19	70	0.225
γ-Al_2O_3-O_2(TRIS)	20	65	0.217
γ-Al_2O_3-PDA-O_2(TRIS)	36	58	0.392
γ-Al_2O_3-O_2(HMTA)	27	56	0.249
γ-Al_2O_3-PDA-O_2(HMTA)	31	60	0.421

As reported in the literature[57], α-Al_2O_3 is thermally stable. There is no weight loss (Figure 23c).

The total weight loss for γ-Al_2O_3 is 6 % (Figure 23d). The first weight loss for γ-Al_2O_3 below 200 °C corresponds to the loss of adsorbed water. The decomposition of PDA begins at 250 °C[58]. The weight loss due to PDA can be calculated by taking the weight loss of α-Al_2O_3-O_2(TRIS) after 250 °C and the weight loss of α-Al_2O_3-PDA-O_2(TRIS) after 250 °C. The difference is due to PDA and is about 0.2 % for α-Al_2O_3-PDA-O_2(TRIS) and 0.9 % for γ-Al_2O_3-PDA-O_2(TRIS).

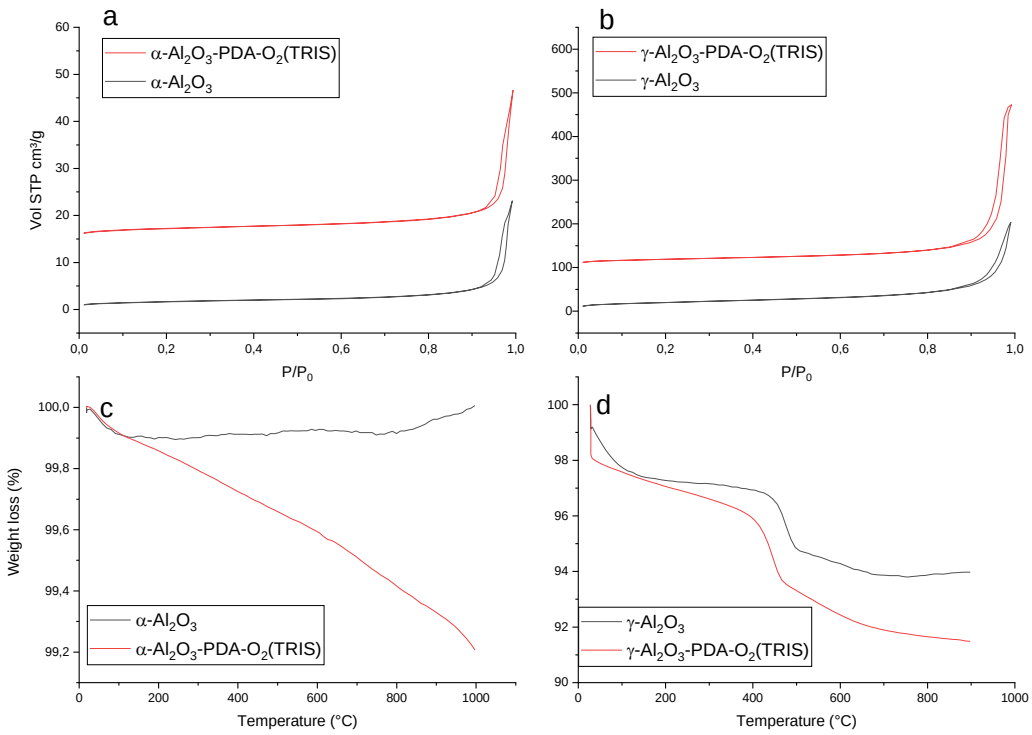

Figure 23: Nitrogen physisorption isotherms of (a) α-Al_2O_3-PDA-O_2(TRIS) and α-Al_2O_3, (b) γ-Al_2O_3-PDA-O_2(TRIS) and γ-Al_2O_3. TGA analysis of (c) α-Al_2O_3 and α-Al_2O_3-PDA-O_2(TRIS), (d) γ-Al_2O_3 and γ-Al_2O_3-PDA-O_2(TRIS).

The XRD pattern for α-Al_2O_3 (Figure 24) is in concordance with the literature[59]. The so called γ-Al_2O_3 (Figure 24) is in fact part γ-Al_2O_3 and part of boehmite(AlOOH)[60]. PDA does not affect the integrity of the support because the diffractogram are the same with PDA or without.

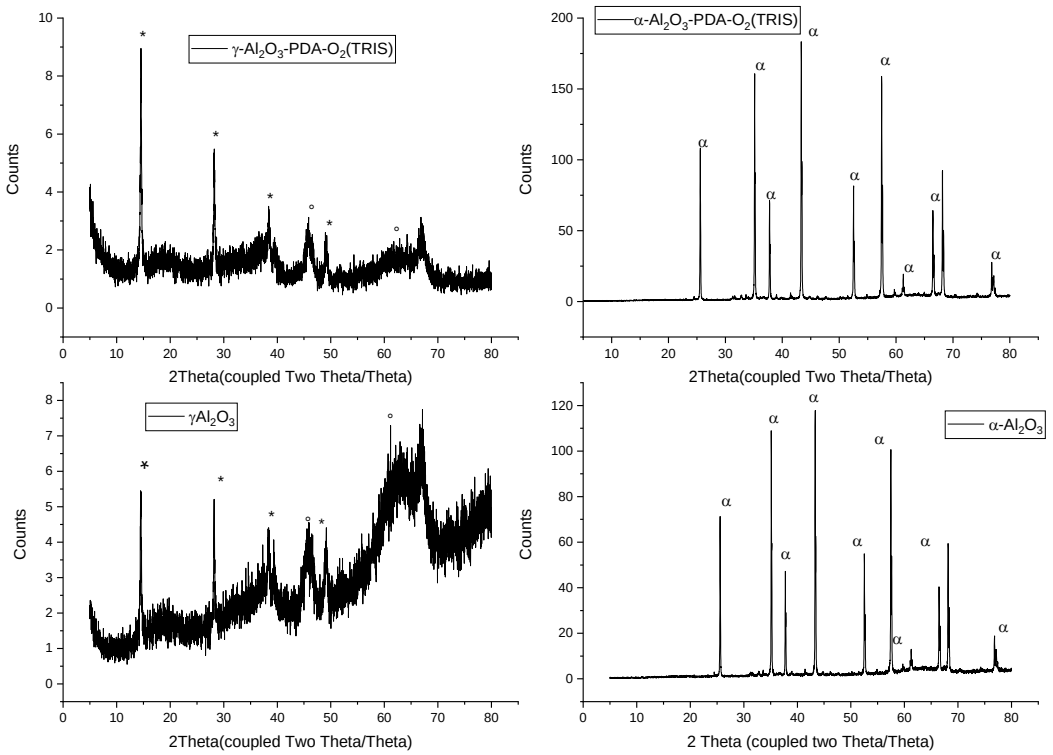

Figure 24: Diffractogram of γ-Al_2O_3-PDA-O_2(TRIS), γ-Al_2O_3, α-Al_2O_3-PDA-O_2(TRIS) and α-Al_2O_3. (*) γ-Al_2O_3 (°) boehmite.

To summarize this section, the deposition of PDA on γ-Al_2O_3 is decreasing the specific area while pore volume and pore diameter are increasing. This may be due to the covering by PDA molecules of the surface of the support in homogeneous layer. In addition, the deposition of PDA on the support leads to a more marked weight loss in TGA analysis due to the thermal degradation of the polymer on the surface support. Finally, the PDA deposition does not affect the integrity of the support as demonstrated shown by XRD.

5.3 Verification of the impregnation of ruthenium and its interaction between Ru and PDA

The XPS survey spectra present a peak Ru3p (Figure 25a). The high resolution Ru 3p spectrum of γ-Al_2O_3-Ru (Figure 25d) shows that Ru3p3/2 is at 462.1 eV which corresponds to a oxidation state of Ru(IV) [61].For γ-Al_2O_3-PDA-O_2(TRIS)-Ru the Ru3p3/2 position is at 462.4 eV(Figure 25e) and for γ-Al_2O_3-PDA-O_2(HMTA) Ru3p3/2 is at 462.2 eV which corresponds also to an oxidation state of Ru(IV). The deconvolution of C1s spectra of γ-Al_2O_3-PDA-O_2(TRIS)-Ru (Figure 25g) and of γ-Al_2O_3-PDA-O_2(HMTA)-Ru (Figure 25h) shows that the ruthenium is present as Ru[III] and as Ru[IV].

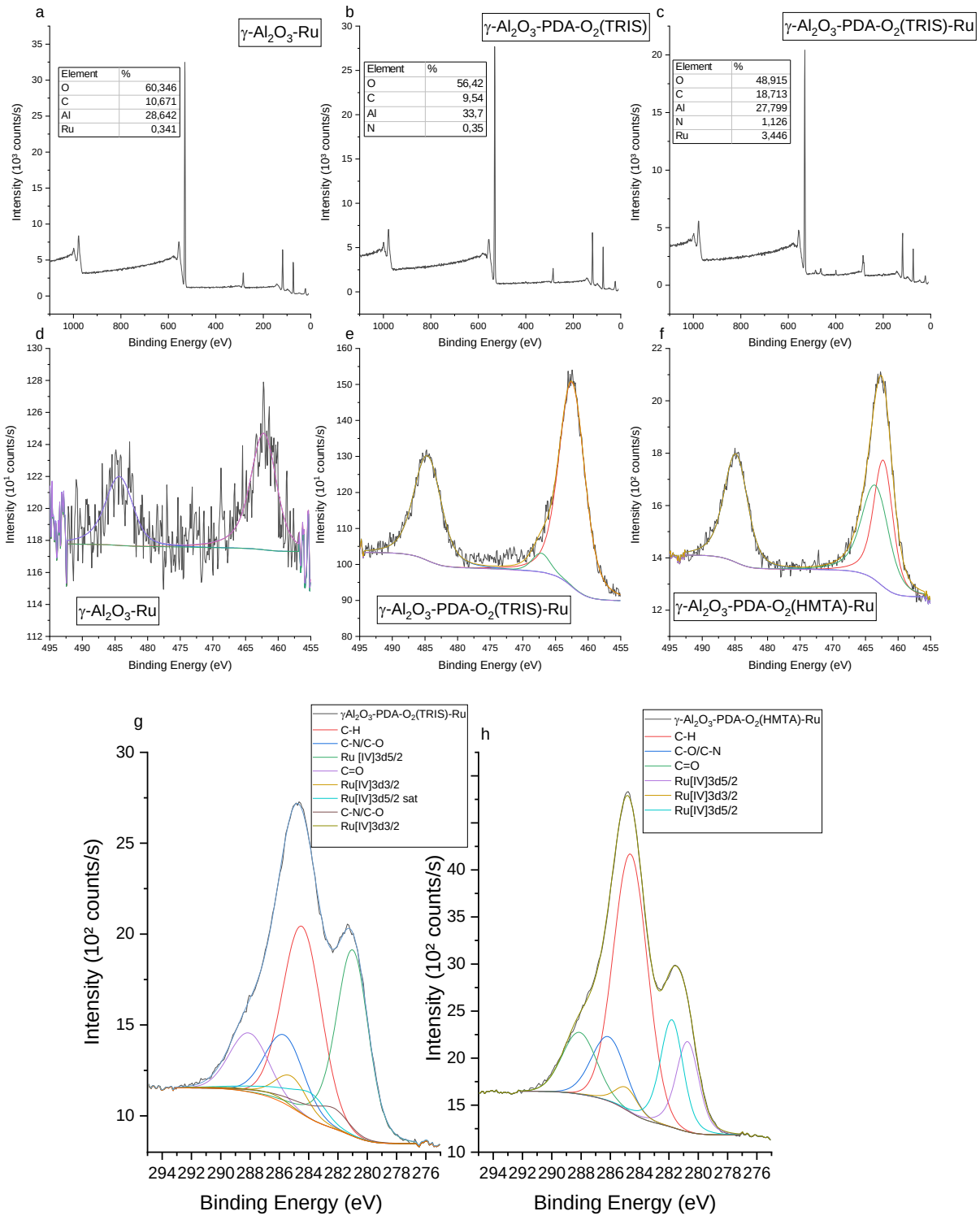

Figure 25:Survey spectra of (a) γ-Al_2O_3-Ru, (b) γ-Al_2O_3-PDA-O_2(TRIS) and (c) γ-Al_2O_3-PDA-O_2(TRIS)-Ru. Deconvoluted Ru3p spectra of (d) γ-Al_2O_3-Ru, (e) γ-Al_2O_3-PDA-O_2(TRIS)-Ru and (f) γ-Al_2O_3-PDA-O_2(HMTA)-Ru. Deconvoluted C1s of (g) γ-Al_2O_3-PDA-O_2(TRIS)-Ru, (h) γ-Al_2O_3-PDA-O_2(HMTA)-Ru.

The impregnation of ruthenium on α-Al_2O_3 and on γ-Al_2O_3 was successful but it leads to a low bulk concentration of ruthenium on the support. But when PDA was deposited on the support before the impregnation it allows to retain ruthenium more abundantly (Table 3).

Table 3: Ru content of γ-Al_2O_3-Ru, γ-Al_2O_3-PDA-O_2(TRIS)-Ru and γ-Al_2O_3-PDA-O_2(HMTA)-Ru measured by ICP-AES.

Sample	Ru loading (Nominal value) (%)	Ru loading (ICP value) (%)
α-Al_2O_3-Ru	2	0.26
γ-Al_2O_3-Ru	2	0.29
γ-Al_2O_3-PDA-O_2(TRIS)-Ru	2	1.96
γ-Al_2O_3-PDA-O_2(HMTA)-Ru	2	1.97

5.4 Catalytic tests

The comparison of α-Al_2O_3 and γ-Al_2O_3 as support for ruthenium was examined. The evaluation of the catalytic performances of both catalysts was assessed by monitoring the conversion (Figure 26a) until 24 hours and the product distribution (and oleic acid) was calculated at t=24 hours (Figure 26b). Catalysts based on γ-Al_2O_3 shows better catalytic activity than those based on α-Al_2O_3 because its specific area is 10 times bigger (Table 2) and a slightly higher Ru loading (Table 3).

The addition of PDA (synthesized either with TRIS or HMTA) improved greatly the catalytic activity in this reaction as making the catalysts reaching 98% of conversion in 24 hours vs 67 % for γ-Al_2O_3-Ru(2%) (Figure 26a). Before reaching 98% at 24 hours γ-Al_2O_3-PDA-O_2(TRIS) has a better conversion than γ-Al_2O_3-PDA-O_2 (HMTA) this is due to a better deposition of PDA with Tris. The addition of PDA whenever it was produced with TRIS or HMTA improved greatly the amount of PA and AA which are the target products. The product distribution of γ-Al_2O_3-PDA-O_2 (TRIS) and γ-Al_2O_3-PDA-O_2 (HMTA) are quite similar.

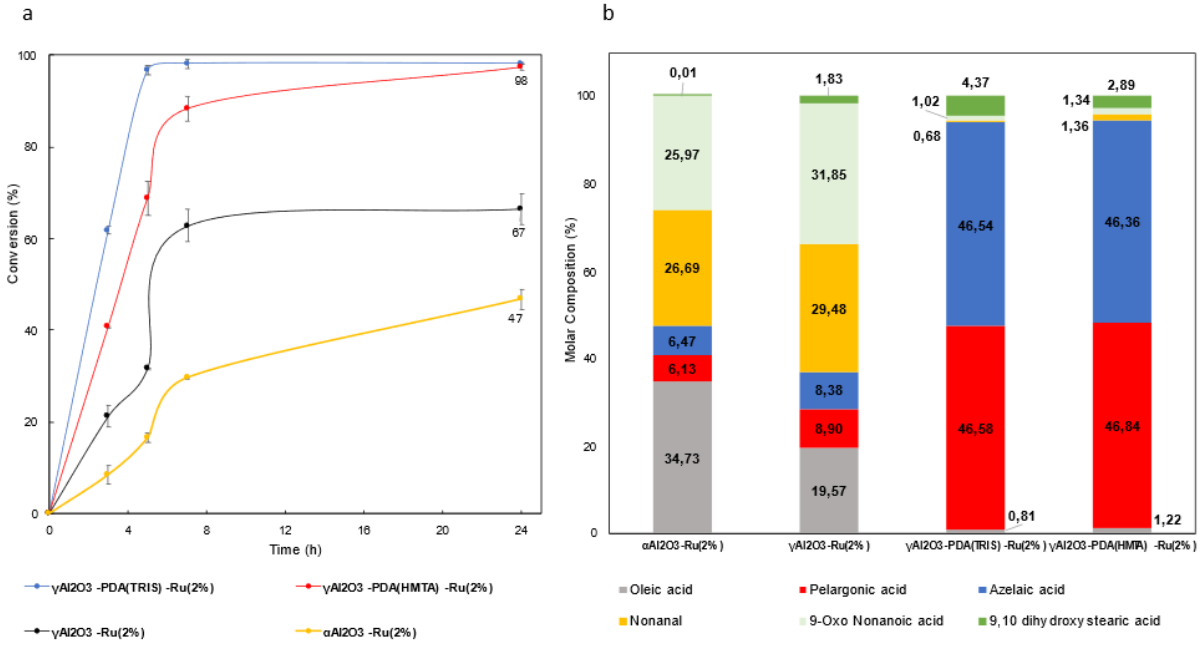

Figure 26:Conversion curves of (a) α-Al_2O_3-Ru(2%), γ-Al_2O_3 -Ru(2%) , γ-Al_2O_3 –PDA-O_2 (TRIS)-Ru(2%) and γ-Al_2O_3-PDA-O_2 (HMTA)-Ru(2%) and products distribution of α-Al_2O_3-Ru, γ-Al_2O_3 -Ru(2%) , γ-Al_2O_3 –PDA-O_2 (TRIS)-Ru(2%) and γ-Al_2O_3-PDA-O_2 (HMTA)-Ru(2%)

Table 4: yields and selectivities of α-Al_2O_3-Ru(2%), γ-Al_2O_3 -Ru(2%) , γ-Al_2O_3 –PDA-O_2 (TRIS)-Ru(2%) and γ-Al_2O_3-PDA-O_2 (HMTA)-Ru(2%)

	Yield		Selectivity	
	PA(%)	AA (%)	PA(%)	AA (%)
α-Al_2O_3-Ru(2%)	9.4	9.9	20.02	21.13
γ-Al_2O_3-Ru(2%)	15.2	14.3	22.9	21.5
γ-Al_2O_3-PDA-O_2 (TRIS)-Ru(2%)	95.9	96.2	97.7	98
γ-Al_2O_3-PDA-O_2 (HMTA)-Ru(2%)	97	97.3	99.6	99.8

5.5 Post-catalytic test characterization

ICP and XPS was performed before and after the catalytic test. After the catalytic test γ-Al_2O_3-Ru(2%) shows no more the XPS ruthenium peak (Figure 27 b) and ICP result shows that there is almost no more ruthenium (Table 5). On the other hand γ-Al_2O_3-PDA-O_2(TRIS)-Ru(2%) and γ-Al_2O_3-PDA-O_2 (HMTA)-Ru(2%) still present a XPS peak for ruthenium after the catalytic test (Figure 27 d,f). Moreover, ICP results show the ability of PDA to retain Ru during the impregnation and avoid a great part of leaching during the catalytic test (Table 5).

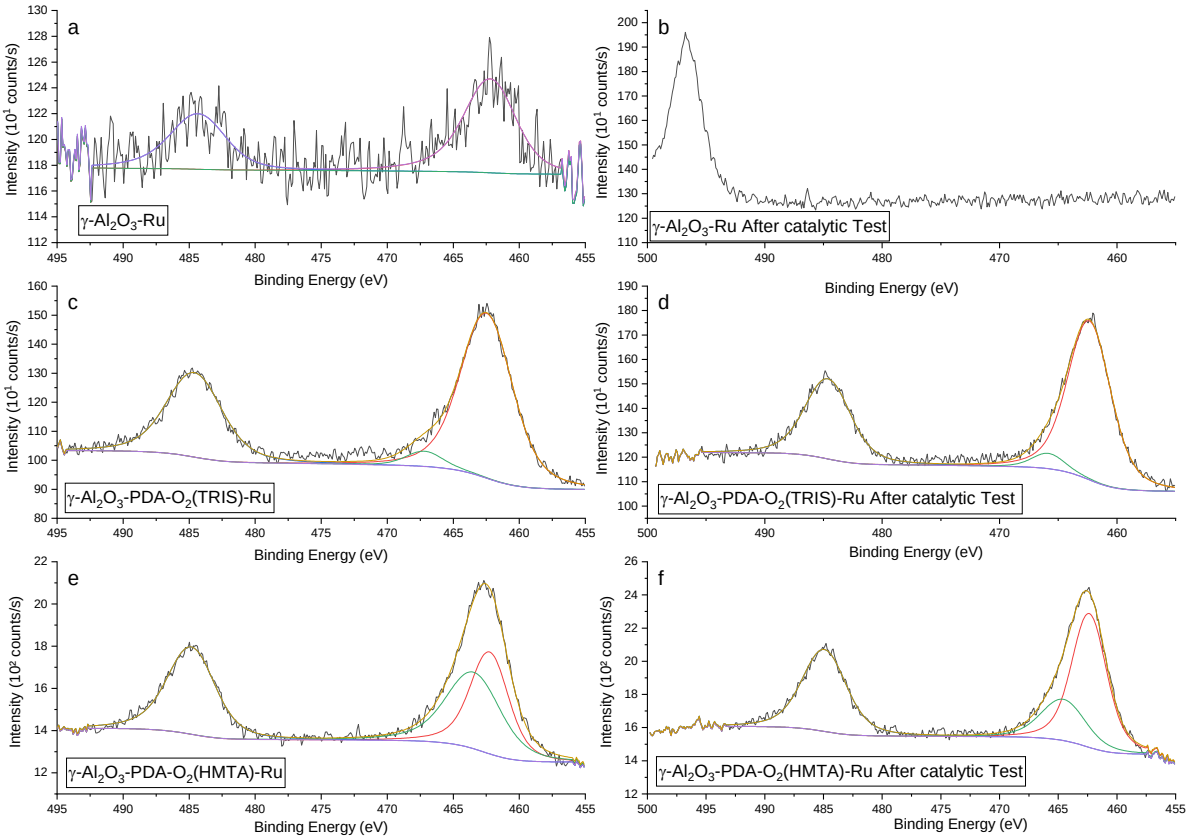

Figure 27: Deconvoluted Ru3p spectra of γ-Al_2O_3-Ru (a) before catalytic test (b) after catalytic test, of γ-Al_2O_3-PDA-O_2(TRIS)-Ru (c) before catalytic test (d) after catalytic test, of γ-Al_2O_3-PDA-O_2(HMTA)-Ru (e) before catalytic test (f) after catalytic test

Table 5:Ru contents before and after catalytic test measured by ICP-AES

Sample	Catalytic test	Ru(% wt.)
α-Al_2O_3-Ru(2%)	Before	0.26
	After	0.02
γ-Al_2O_3-Ru(2%)	Before	0.29
	After	0.02
γ-Al_2O_3-PDA-O_2(TRIS)-Ru(2%)	Before	1.96
	After	1.91
γ-Al_2O_3-PDA-O_2(HMTA)-Ru(2%)	Before	1.97
	After	1.82

The conversion decreased significantly at the first recycle run for α-Al_2O_3-Ru(2%) and γ-Al_2O_3-Ru(2%)(Figure 28a,b).This can be explained because of the leaching of ruthenium during the catalytic test as ICP results have shown.

For γ-Al_2O_3-PDA-O_2(TRIS)-Ru(2%) and γ-Al_2O_3-PDA-O_2(HMTA)-Ru(2%), the conversion curve was quite similar at least until the 3 recycle tests. (Figure 28c,d) γ-Al_2O_3-PDA-O_2(TRIS)-Ru(2%) shows a better robustness than γ-Al_2O_3-PDA-O_2(HMTA)-Ru(2%) for the 4 and 5 recycle tests. This may be due to a better deposition of PDA and thus a better capacity than γ-Al_2O_3-PDA-O_2(HMTA)-Ru(2%) to retain Ru longer on the composite.

γ-Al_2O_3-PDA-O_2(TRIS)-Ru(2%) and γ-Al_2O_3-PDA-O_2(HMTA)-Ru(2%) have an increase of conversion even when the solid catalyst is removed. This results from active Ru species dissolved in the reaction medium because of the leaching of ruthenium (Figure 28). The recycling tests show that γ-Al_2O_3-PDA-O_2(TRIS)-Ru(2%) and γ-Al_2O_3-PDA-O_2(HMTA)-Ru(2%) are keeping their activity at least during the first 3 cycles but the "Hot-centrifugation" test shows that there are some leaching of ruthenium during the catalytic test. This result can be explained by the fact that the catalyst when PDA is present behaves in fact as a boomerang catalyst[62]. The actives species, in this case ruthenium[III], on the support (γ-Al_2O_3) will be released when put in contact with $NaIO_4$ and become RuO_4. After the oxidative cleavage of oleic acid, the composite recovered its Ru ions thanks to PDA which can chelate Ru species by forming a complex with them.

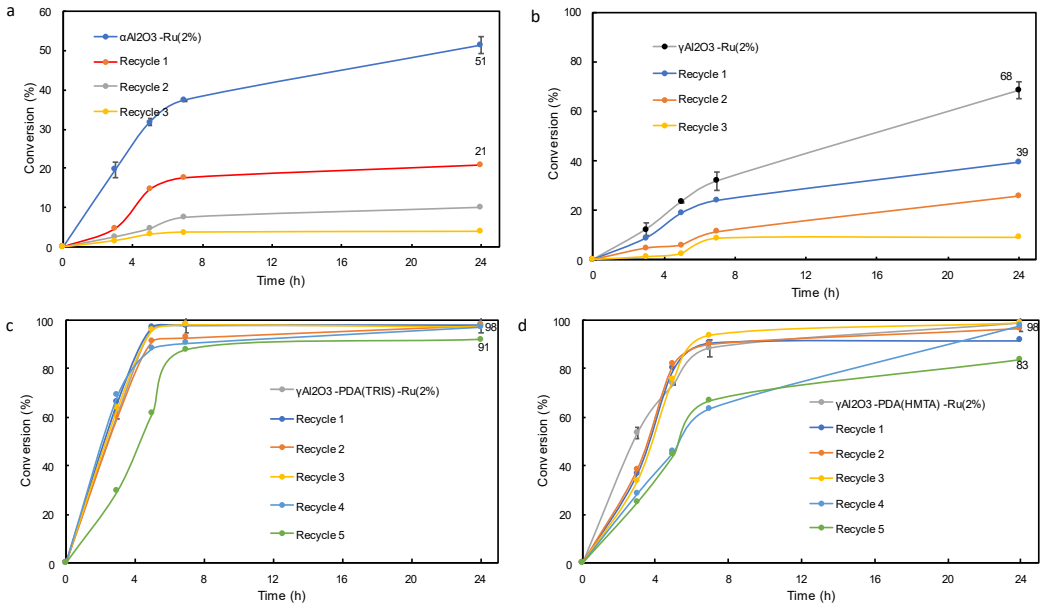

Figure 28:Conversion curve during the recycle tests of α-Al_2O_3-Ru(2%), γ-Al_2O_3 -Ru(2%) , γ-Al_2O_3 –PDA-O_2 (TRIS)-Ru(2%) and γ-Al_2O_3-PDA-O_2 (HMTA)-Ru(2%)

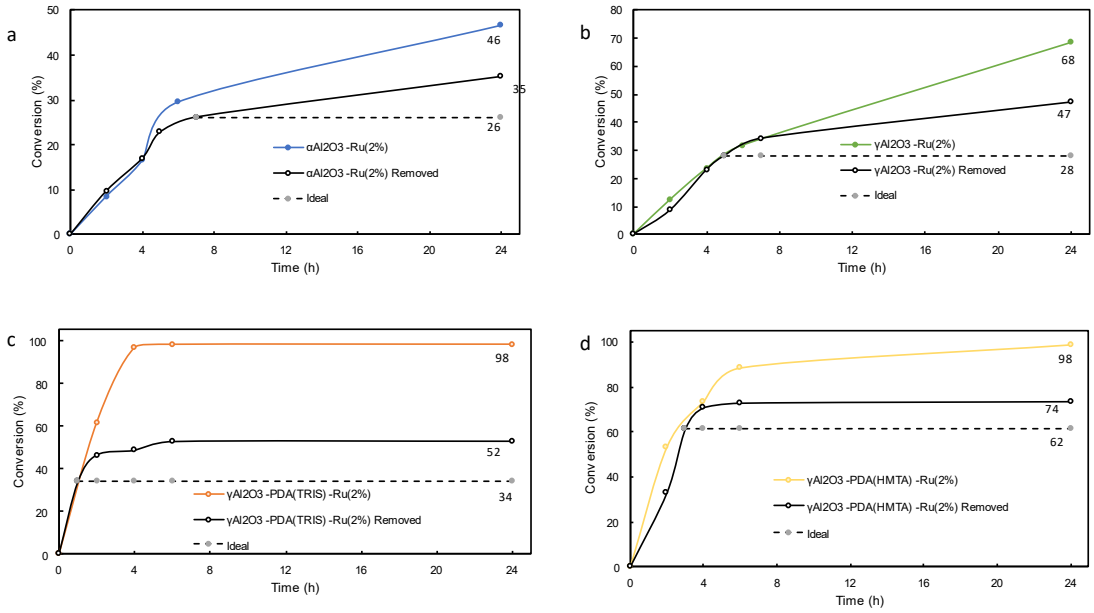

Figure 29:Conversion curves of α-Al_2O_3-Ru(2%), γ-Al_2O_3 -Ru(2%), γ-Al_2O_3 –PDA-O_2 (TRIS)-Ru(2%) and γ-Al_2O_3-PDA-O_2 (HMTA)-Ru(2%) . The dotted line represents the conversion at which the solid particle was removed from the medium.

6 Conclusion and future works

For α-Al_2O_3 and γ-Al_2O_3 the deposition of PDA was successful when oxygen was present in alkaline solution. The presence of PDA was difficult to detect on α-Al_2O_3 because the amount of dopamine required to form a monolayer was very small due to the low specific surface area. The Tris buffer led to a higher deposition of PDA on the support than HMTA because Tris adjusts the pH at 8. It was expected that the decomposition of HMTA, which releases ammonia would trigger the polymerization, but it was no sufficient to reach a pH of 8. For further work it will be interesting to see the impact of the deposition of PDA with Tris and HMTA.

The support which contains PDA shows a higher content of ruthenium after the impregnation due to the ability of PDA to form a complex with Ru ions. Therefore, there are very active with high conversion and selectivity towards PA and AA.

The "hot centrifugation" tests demonstrated the presence of active ruthenium species dissolved in the reaction medium. Indeed, the conversion kept increasing even after removing the solid catalyst. The leaching of Ru was confirmed by ICP.

Surprisingly, the recyclability test displays that γ-Al_2O_3-PDA-O_2(TRIS)-Ru(2%) retains its activity during 4 recycle tests and γ-Al_2O_3-PDA-O_2(HMTA)-Ru(2%) during 3 recycle tests. This leads to the conclusion that the catalyst is in fact a boomerang catalyst which combines the benefits of heterogenous and homogeneous catalysis. [62]

During this work, the benefit of PDA has been clearly demonstrated. However,the nature of the interactions between PDA and the alumina, and between PDA and ruthenium remains unclear and would need to be further examined.

References

(1) Metzger, J. O.; Eissen, M. Concepts on the Contribution of Chemistry to a Sustainable Development. Renewable Raw Materials. *Comptes Rendus Chim.* **2004**, *7* (6), 569–581. https://doi.org/10.1016/j.crci.2003.12.003.

(2) Kerenkan, A. E.; Béland, F.; Do, T.-O. Chemically Catalyzed Oxidative Cleavage of Unsaturated Fatty Acids and Their Derivatives into Valuable Products for Industrial Applications: A Review and Perspective. *Catal. Sci. Technol.* **2016**, *6* (4), 971–987. https://doi.org/10.1039/C5CY01118C.

(3) Orellana-Coca, C.; Adlercreutz, D.; Andersson, M. M.; Mattiasson, B.; Hatti-Kaul, R. Analysis of Fatty Acid Epoxidation by High Performance Liquid Chromatography Coupled with Evaporative Light Scattering Detection and Mass Spectrometry. *Chem. Phys. Lipids* **2005**, *135* (2), 189–199. https://doi.org/10.1016/j.chemphyslip.2005.02.014.

(4) *Selective hydrogenation of fatty acids and methyl esters of fatty acids to obtain fatty alcohols–a review - Sánchez - 2017 - Journal of Chemical Technology & Biotechnology - Wiley Online Library*. https://onlinelibrary.wiley.com/doi/10.1002/jctb.5039 (accessed 2022-05-16).

(5) Spannring, P.; Bruijnincx, P. C. A.; Weckhuysen, B. M.; Gebbink, R. J. M. K. Transition Metal-Catalyzed Oxidative Double Bond Cleavage of Simple and Bio-Derived Alkenes and Unsaturated Fatty Acids. *Catal. Sci. Technol.* **2014**, *4* (8), 2182–2209. https://doi.org/10.1039/C3CY01095C.

(6) De Leon Izeppi, G. A.; Dubois, J.-L.; Balle, A.; Soutelo-Maria, A. Economic Risk Assessment Using Monte Carlo Simulation for the Production of Azelaic Acid and Pelargonic Acid from Vegetable Oils. *Ind. Crops Prod.* **2020**, *150*, 112411. https://doi.org/10.1016/j.indcrop.2020.112411.

(7) Karmakar, G.; Ghosh, P.; Kohli, K.; Sharma, B.; Erhan, S. Chemicals from Vegetable Oils, Fatty Derivatives, and Plant Biomass; 2020; pp 1–31. https://doi.org/10.1021/bk-2020-1347.ch001.

(8) Anneken, D. J.; Both, S.; Christoph, R.; Fieg, G.; Steinberner, U.; Westfechtel, A. Fatty Acids. In *Ullmann's Encyclopedia of Industrial Chemistry*; John Wiley & Sons, Ltd, 2006. https://doi.org/10.1002/14356007.a10_245.pub2.

(9) Warwel, S.; Sojka, M.; Klaas, M. R. gen. Synthesis of Dicarboxylic Acids by Transition-Metal Catalyzed Oxidative Cleavage of Terminal-Unsaturated Fatty Acids. In *Organic Peroxygen Chemistry*; Herrmann, W. A., Ed.; Topics in Current Chemistry; Springer: Berlin, Heidelberg, 1993; pp 79–98. https://doi.org/10.1007/3-540-56252-4_26.

(10) *Oxidation of unsaturated fatty acids with ruthenium and osmium tetroxide - Foglia - 1977 - Journal of the American Oil Chemists' Society - Wiley Online Library*. https://aocs.onlinelibrary.wiley.com/doi/abs/10.1007/BF02909058 (accessed 2022-03-06).

(11) Zimmermann, F.; Meux, E.; Mieloszynski, J.-L.; Lecuire, J.-M.; Oget, N. Ruthenium Catalysed Oxidation without CCl 4 of Oleic Acid, Other Monoenic Fatty Acids and Alkenes. *Tetrahedron Lett. - TETRAHEDRON LETT* **2005**, *46*, 3201–3203. https://doi.org/10.1016/j.tetlet.2005.03.052.

(12) *The ultrasound-assisted oxidative scission of monoenic fatty acids by ruthenium tetroxide catalysis: Influence of the mixture of solvents - ScienceDirect*. https://www.sciencedirect.com/science/article/pii/S1350417708001302 (accessed 2021-11-01).

(13) Behr, A.; Tenhumberg, N.; Wintzer, A. Efficient Ruthenium-Catalysed Oxidative Cleavage of Methyl Oleate with Hydrogen Peroxide as Oxidant. *RSC Adv.* **2012**, *3* (1), 172–180. https://doi.org/10.1039/C2RA22370H.

(14) Ho, C.-M.; Yu, W.-Y.; Che, C.-M. Ruthenium Nanoparticles Supported on Hydroxyapatite as an Efficient and Recyclable Catalyst for Cis-Dihydroxylation and Oxidative Cleavage of Alkenes. *Angew. Chem. Int. Ed Engl.* **2004**, *43* (25), 3303–3307. https://doi.org/10.1002/anie.200453703.

(15) Guicheret, B.; Da Silva, E.; Philippe, R.; Favre-Reguillon, A.; Vanoye, L.; Blach, P.; Raoul, Y.; De Bellefon, C.; Métay, E.; Lemaire, M. Aerobic Oxidative Cleavage of Vicinal Diol Fatty Esters by a Supported Ruthenium Hydroxide Catalyst. *ACS Sustain. Chem. Eng.* **2020**, *8* (35), 13167–13175. https://doi.org/10.1021/acssuschemeng.0c01265.

(16) Papafotiou, F.; Karidi, K.; Garoufis, A.; Louloudi, M. Covalent Attachment of a Biomimetic Ru-(Terpy)(Bpy) Complex on Silica Surface: Catalytic Potential. *Polyhedron* **2013**, *52*, 634. https://doi.org/10.1016/j.poly.2012.07.094.
(17) *Mesoporous silica as phase transfer agent in the biphasic oxidative cleavage of alkenes using triazole complexes of ruthenium as catalyst precursors | Semantic Scholar*. https://www.semanticscholar.org/paper/Mesoporous-silica-as-phase-transfer-agent-in-the-of-Leckie-Mapolie/da132c9fbd6c7f23575eed3f9fd42ded1dddb230 (accessed 2022-04-06).
(18) Saiz-Poseu, J.; Mancebo-Aracil, J.; Nador, F.; Busqué, F.; Ruiz-Molina, D. The Chemistry behind Catechol-Based Adhesion. *Angew. Chem. Int. Ed.* **2019**, *58* (3), 696–714. https://doi.org/10.1002/anie.201801063.
(19) Barclay, T.; Hegab, H.; Clarke, S.; Ginic-Markovic, M. Versatile Surface Modification Using Polydopamine and Related Polycatecholamines: Chemistry, Structure, and Applications. *Adv. Mater. Interfaces* **2017**, *4*, 1601192. https://doi.org/10.1002/admi.201601192.
(20) Lee, H.; Dellatore, S. M.; Miller, W. M.; Messersmith, P. B. Mussel-Inspired Surface Chemistry for Multifunctional Coatings. *Science* **2007**, *318* (5849), 426–430. https://doi.org/10.1126/science.1147241.
(21) *Non-Covalent Self-Assembly and Covalent Polymerization Co-Contribute to Polydopamine Formation - Hong - 2012 - Advanced Functional Materials - Wiley Online Library*. https://onlinelibrary.wiley.com/doi/abs/10.1002/adfm.201201156 (accessed 2022-01-25).
(22) *Degree of polymerization of 5,6-dihydroxyindole-derived eumelanin from chemical degradation study - Okuda - 2014 - Pigment Cell & Melanoma Research - Wiley Online Library*. https://onlinelibrary.wiley.com/doi/full/10.1111/pcmr.12254 (accessed 2022-01-25).
(23) Chen, C.-T.; Martin-Martinez, F. J.; Jung, G. S.; Buehler, M. J. Polydopamine and Eumelanin Molecular Structures Investigated with Ab Initio Calculations. *Chem. Sci.* **2017**, *8* (2), 1631–1641. https://doi.org/10.1039/C6SC04692D.
(24) Liebscher, J.; Mrówczyński, R.; Scheidt, H. A.; Filip, C.; Hădade, N. D.; Turcu, R.; Bende, A.; Beck, S. Structure of Polydopamine: A Never-Ending Story? *Langmuir ACS J. Surf. Colloids* **2013**, *29* (33), 10539–10548. https://doi.org/10.1021/la4020288.
(25) Dreyer, D. R.; Miller, D. J.; Freeman, B. D.; Paul, D. R.; Bielawski, C. W. Elucidating the Structure of Poly(Dopamine). *Langmuir* **2012**, *28* (15), 6428–6435. https://doi.org/10.1021/la204831b.
(26) Della Vecchia, N. F.; Avolio, R.; Alfè, M.; Errico, M. E.; Napolitano, A.; d'Ischia, M. Building-Block Diversity in Polydopamine Underpins a Multifunctional Eumelanin-Type Platform Tunable Through a Quinone Control Point. *Adv. Funct. Mater.* **2013**, *23* (10), 1331–1340. https://doi.org/10.1002/adfm.201202127.
(27) Lakshminarayanan, R.; Madhavi, S.; Sim, C. P. C. *Oxidative Polymerization of Dopamine: A High-Definition Multifunctional Coatings for Electrospun Nanofibers - An Overview*; IntechOpen, 2018. https://doi.org/10.5772/intechopen.81036.
(28) Klosterman, L. J. Deposition, Oxidation, and Adhesion Mechanisms of Conformal Polydopamine Films. thesis, Carnegie Mellon University, 2016. https://doi.org/10.1184/R1/6715727.v1.
(29) *Tris Buffer Modulates Polydopamine Growth, Aggregation, and Paramagnetic Properties | Langmuir*. https://pubs.acs.org/doi/10.1021/la501560z (accessed 2021-03-14).
(30) Wu, C.; Zhang, G.; Xia, T.; Li, Z.; Zhao, K.; Deng, Z.; Guo, D.; Peng, B. Bioinspired Synthesis of Polydopamine/Ag Nanocomposite Particles with Antibacterial Activities. *Mater. Sci. Eng. C Mater. Biol. Appl.* **2015**, *55*, 155–165. https://doi.org/10.1016/j.msec.2015.05.032.
(31) Liu, Y.; Ai, K.; Liu, J.; Deng, M.; He, Y.; Lu, L. Dopamine-Melanin Colloidal Nanospheres: An Efficient Near-Infrared Photothermal Therapeutic Agent for In Vivo Cancer Therapy. *Adv. Mater.* **2013**, *25* (9), 1353–1359. https://doi.org/10.1002/adma.201204683.
(32) Lin, J.-H.; Yu, C.-J.; Yang, Y.-C.; Tseng, W.-L. Formation of Fluorescent Polydopamine Dots from Hydroxyl Radical-Induced Degradation of Polydopamine Nanoparticles. *Phys. Chem. Chem. Phys.* **2015**, *17* (23), 15124–15130. https://doi.org/10.1039/C5CP00932D.

(33) *Oxygen Concentration Control of Dopamine-Induced High Uniformity Surface Coating Chemistry | ACS Applied Materials & Interfaces*. https://pubs.acs.org/doi/10.1021/am302439g (accessed 2022-01-31).
(34) Ball, V.; Frari, D. D.; Toniazzo, V.; Ruch, D. Kinetics of Polydopamine Film Deposition as a Function of PH and Dopamine Concentration: Insights in the Polydopamine Deposition Mechanism. *J. Colloid Interface Sci.* **2012**, *386* (1), 366–372. https://doi.org/10.1016/j.jcis.2012.07.030.
(35) Alfieri, M. L.; Panzella, L.; Oscurato, S. L.; Salvatore, M.; Avolio, R.; Errico, M. E.; Maddalena, P.; Napolitano, A.; D'Ischia, M. The Chemistry of Polydopamine Film Formation: The Amine-Quinone Interplay. *Biomimetics* **2018**, *3* (3), 26. https://doi.org/10.3390/biomimetics3030026.
(36) *Polydopamine Ultrathin Film Growth on Mica via In-Situ Polymerization of Dopamine with Applications for Silver-Based Antimicrobial Coatings - PubMed*. https://pubmed.ncbi.nlm.nih.gov/33535625/ (accessed 2022-03-23).
(37) Hadouchi, S. E. Y.-E. Control of the Structure and the Properties of Polydopamine in Suspensions, in Films and in Gels for Biomedical Applications. phdthesis, Université de Strasbourg, 2020.
(38) Mian, S. A.; Yang, L.-M.; Saha, L. C.; Ahmed, E.; Ajmal, M.; Ganz, E. A Fundamental Understanding of Catechol and Water Adsorption on a Hydrophilic Silica Surface: Exploring the Underwater Adhesion Mechanism of Mussels on an Atomic Scale. *Langmuir* **2014**, *30* (23), 6906–6914. https://doi.org/10.1021/la500800f.
(39) Martin, S. T.; Kesselman, J. M.; Park, D. S.; Lewis, N. S.; Hoffmann, M. R. Surface Structures of 4-Chlorocatechol Adsorbed on Titanium Dioxide. *Environ. Sci. Technol.* **1996**, *30* (8), 2535–2542. https://doi.org/10.1021/es950872e.
(40) Syres, K.; Thomas, A.; Bondino, F.; Malvestuto, M.; Grätzel, M. Dopamine Adsorption on Anatase TiO2(101): A Photoemission and NEXAFS Spectroscopy Study. *Langmuir ACS J. Surf. Colloids* **2010**, *26* (18), 14548–14555. https://doi.org/10.1021/la1016092.
(41) Yu, J.; Wei, W.; Menyo, M. S.; Masic, A.; Waite, J. H.; Israelachvili, J. N. Adhesion of Mussel Foot Protein-3 to TiO2 Surfaces: The Effect of PH. *Biomacromolecules* **2013**, *14* (4), 1072–1077. https://doi.org/10.1021/bm301908y.
(42) Qin, Z.; Buehler, M. Molecular Mechanics of Dihydroxyphenylalanine at a Silica Interface. *Appl. Phys. Lett.* **2012**, *101* (8), 083702. https://doi.org/10.1063/1.4747214.
(43) McBride, M. B.; Wesselink, L. G. Chemisorption of Catechol on Gibbsite, Boehmite, and Noncrystalline Alumina Surfaces. *Environ. Sci. Technol.* **1988**, *22* (6), 703–708. https://doi.org/10.1021/es00171a014.
(44) *Chemistry of Polydopamine – Scope, Variation, and Limitation - Liebscher - 2019 - European Journal of Organic Chemistry - Wiley Online Library*. https://chemistry-europe.onlinelibrary.wiley.com/doi/abs/10.1002/ejoc.201900445?af=R (accessed 2021-11-28).
(45) *Benzene hydrogenation over polydopamine-modified MCM-41 supported Ruthenium-Lanthanum catalyst: Inorganic and Nano-Metal Chemistry: Vol 48, No 12*. https://www.tandfonline.com/doi/abs/10.1080/24701556.2019.1567539 (accessed 2022-03-24).
(46) Holten-Andersen, N.; Harrington, M. J.; Birkedal, H.; Lee, B. P.; Messersmith, P. B.; Lee, K. Y. C.; Waite, J. H. PH-Induced Metal-Ligand Cross-Links Inspired by Mussel Yield Self-Healing Polymer Networks with near-Covalent Elastic Moduli. *Proc. Natl. Acad. Sci.* **2011**, *108* (7), 2651–2655. https://doi.org/10.1073/pnas.1015862108.
(47) *Polydopamine and Its Derivative Materials: Synthesis and Promising Applications in Energy, Environmental, and Biomedical Fields | Chemical Reviews*. https://pubs.acs.org/doi/10.1021/cr400407a (accessed 2022-04-06).
(48) Carstens, S.; Meyer, R.; Enke, D. Towards Macroporous α-Al2O3—Routes, Possibilities and Limitations. *Materials* **2020**, *13* (7), 1787. https://doi.org/10.3390/ma13071787.
(49) Yu, X.-H.; Zhao, Z.-Y.; Yi, J.-L.; Wang, F.-Y.; Zhang, R.-L.; Yu, Q.; Liu, L. Nitrogen-Doped Hollow Carbon Spheres from Bio-Inspired Dopamine: Hexamethylenetetramine-Induced

Polymerization, Morphology Control and Supercapacitor Performance. *J. Electroanal. Chem.* **2021**, *900*, 115735. https://doi.org/10.1016/j.jelechem.2021.115735.
(50) Kubicki, J.; Apitz, S. Molecular Cluster Models of Aluminum Oxide and Aluminum Hydroxide Surfaces. *Am. Mineral.* **1998**, *83*, 1054–1066. https://doi.org/10.2138/am-1998-9-1014.
(51) Bernsmann, F.; Ersen, O.; Voegel, J.-C.; Jan, E.; Kotov, N. A.; Ball, V. Melanin-Containing Films: Growth from Dopamine Solutions versus Layer-by-Layer Deposition. *Chemphyschem Eur. J. Chem. Phys. Phys. Chem.* **2010**, *11* (15), 3299–3305. https://doi.org/10.1002/cphc.201000384.
(52) Cruickshank, L.; Kennedy, A. R.; Shankland, N. Tautomeric and Ionisation Forms of Dopamine and Tyramine in the Solid State. *J. Mol. Struct.* **2013**, *1051*, 132–136. https://doi.org/10.1016/j.molstruc.2013.08.002.
(53) Martínez-Huitle, C. A.; Cerro-Lopez, M.; Quiroz, M. A. Electrochemical Behaviour of Dopamine at Covalent Modified Glassy Carbon Electrode with L-Cysteine: Preliminary Results. *Mater. Res.* **2009**, *12* (4), 375–384. https://doi.org/10.1590/S1516-14392009000400002.
(54) Santhiya, D.; Subramanian, S.; Natarajan, K. A.; Malghan, S. G. Surface Chemical Studies on Alumina Suspensions Using Ammonium Poly(Methacrylate). *Colloids Surf. Physicochem. Eng. Asp.* **2000**, *2–3* (164), 143–154.
(55) Rutkowska, I.; Marchewka, J.; Jeleń, P.; Odziomek, M.; Korpyś, M.; Paczkowska, J.; Sitarz, M. Chemical and Structural Characterization of Amorphous and Crystalline Alumina Obtained by Alternative Sol–Gel Preparation Routes. *Materials* **2021**, *14* (7), 1761. https://doi.org/10.3390/ma14071761.
(56) Kajama, M. Hydrogen Permeation Using Nanostructured Silica Membranes; 2015; pp 447–456. https://doi.org/10.2495/SDP150381.
(57) Amrute, A. P.; Jeske, K.; Łodziana, Z.; Prieto, G.; Schüth, F. Hydrothermal Stability of High-Surface-Area α-Al2O3 and Its Use as a Support for Hydrothermally Stable Fischer–Tropsch Synthesis Catalysts. *Chem. Mater.* **2020**, *32* (10), 4369–4374. https://doi.org/10.1021/acs.chemmater.0c01587.
(58) Shapter, J.; Popelka-Filcoff, R.; Bennett, J.; Ellis, A. Copper Removal Using Bio-Inspired Polydopamine Coated Natural Zeolites. *J. Hazard. Mater.* **2014**, *273C*, 174–182. https://doi.org/10.1016/j.jhazmat.2014.03.048.
(59) Mulpur, P.; Lingam, K.; Chunduri, A.; Rattan, T.; Rao, A.; Kamisetti, V. Surface Plasmon Coupled Emission Studies on Engineered Thin Film Hybrids of Nano Alpha-Al2O3 on Silver. **2013**, *1576*. https://doi.org/10.1063/1.4861970.
(60) Sifontes, A.; Gutiérrez, B.; Mónaco, A.; Yanez, A.; Diaz, Y.; Mendez, F.; Llovera, L.; Cañizales, E.; Brito, J. Preparation of Funcionalized Porous Nano-γ-Al2O3 Powders Employing Colophony Extract. *Biotechnol. Rep.* **2014**, *4*, 21–29. https://doi.org/10.1016/j.btre.2014.07.001.
(61) Morgan, D. J. Resolving Ruthenium: XPS Studies of Common Ruthenium Materials. *Surf. Interface Anal.* **2015**, *47* (11), 1072–1079. https://doi.org/10.1002/sia.5852.
(62) Gámez, S.; de la Torre, E.; Gaigneaux, E. M. Carbon Black-Polydopamine-Ruthenium Composite as a Recyclable Boomerang Catalyst for the Oxidative Cleavage of Oleic Acid. *Chem. Eng. J.* **2022**, *427*, 131820. https://doi.org/10.1016/j.cej.2021.131820.

Appendices

Supplementary figures

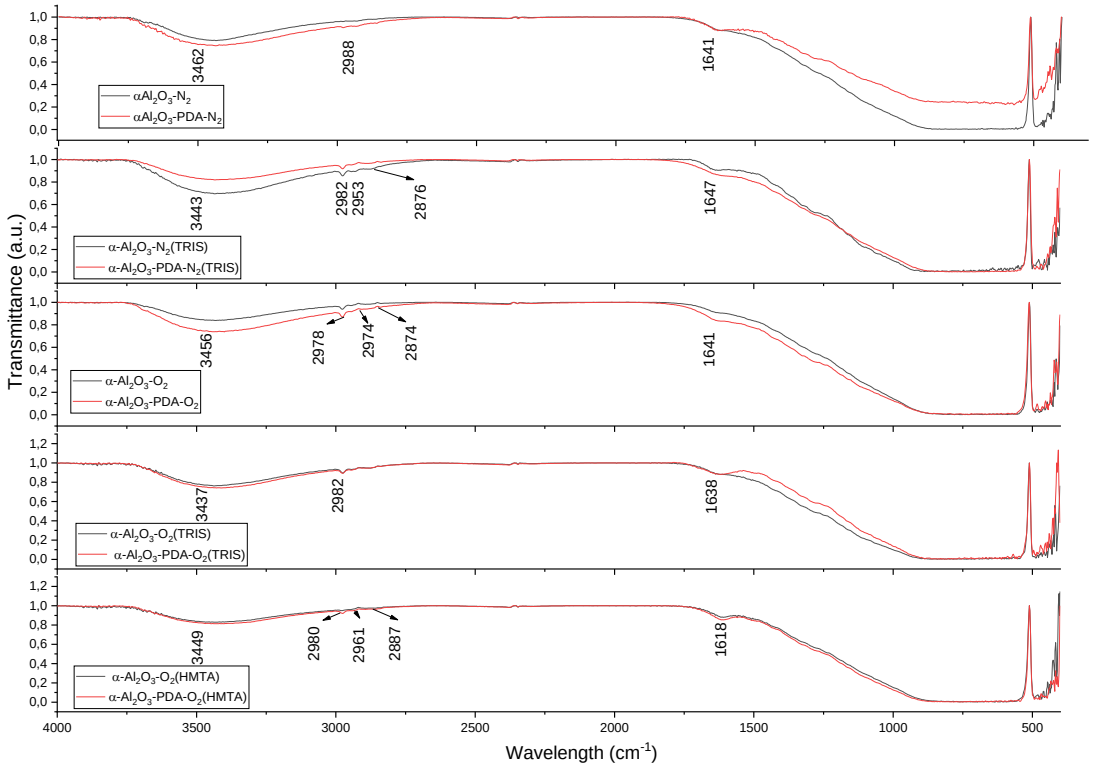

Figure 30: Fourier-transform spectrum of α-Al_2O_3-PDA-N_2, α-Al_2O_3-N_2, α-Al_2O_3-PDA-N_2(TRIS) , α-Al_2O_3-N_2(TRIS), α-Al_2O_3-PDA-O_2, α-Al_2O_3-O_2, α-Al_2O_3-PDA-O_2(TRIS), α-Al_2O_3-O_2(TRIS), α-Al_2O_3-PDA-O_2(HMTA) and α-Al_2O_3-O_2(HMTA).

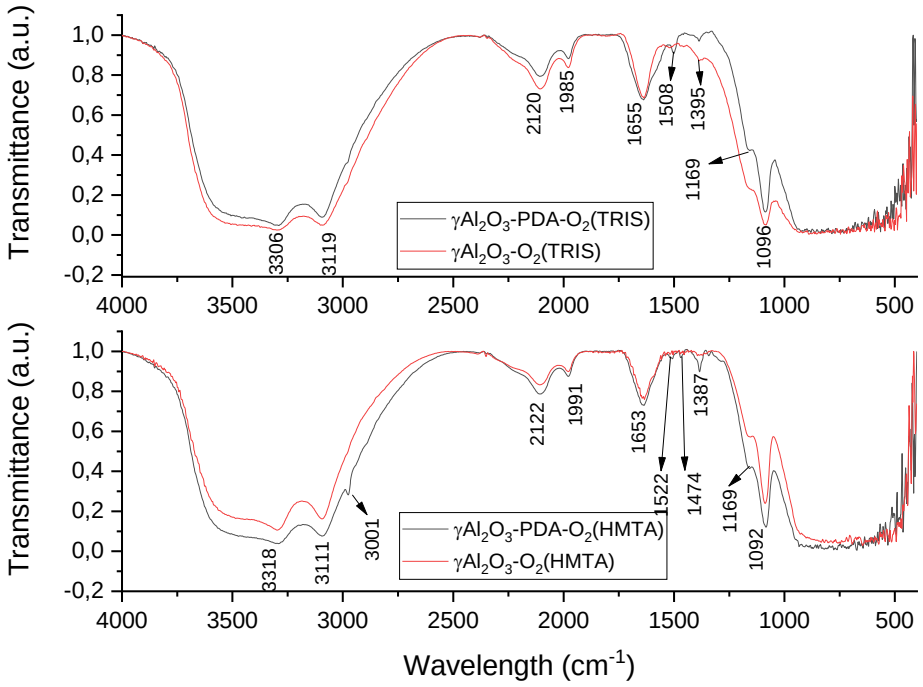

Figure 31: FTIR spectra of γ-Al_2O_3-O_2(TRIS) , γ-Al_2O_3-PDA-O_2(TRIS), γ-Al_2O_3-O_2(HMTA) and γ-Al_2O_3-PDA-O_2(HMTA)

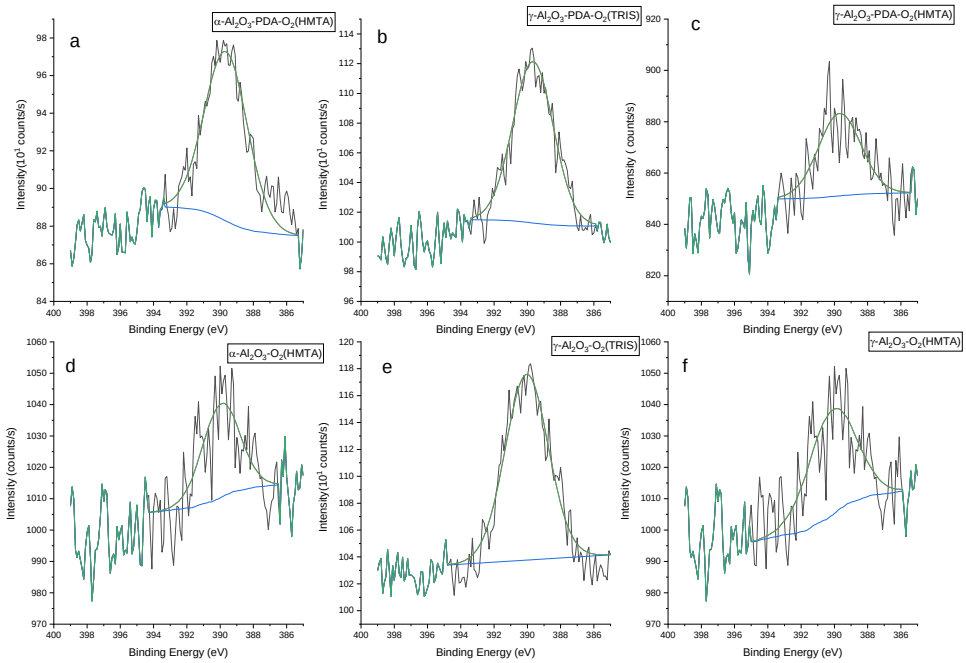

Figure 32: High resolution spectra N1s of(a) α-Al_2O_3-PDA-O_2(HMTA), (b) γ-Al_2O_3-PDA-O_2(TRIS),(c) γ-Al_2O_3-PDA-O_2(HMTA), (d) α-Al_2O_3-O_2(HMTA), (e) γ-Al_2O_3-O_2(TRIS) and (f)) γ-Al_2O_3-O_2(HMTA).

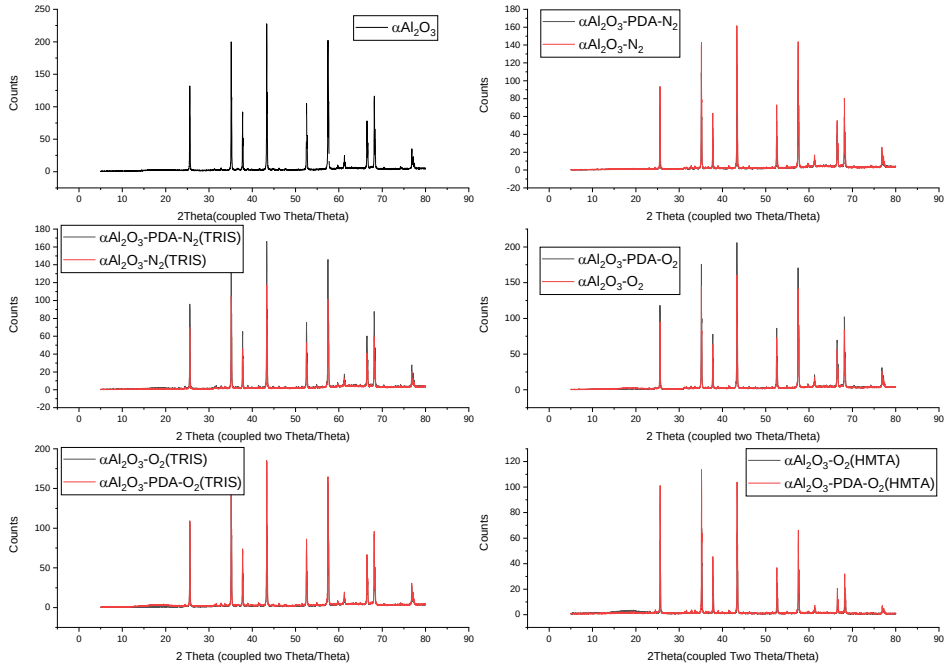

Figure 33: XRD pattern of α-Al_2O_3 and of α-Al_2O_3-PDA-N_2, α-Al_2O_3-N_2, α-Al_2O_3-PDA-N_2(TRIS) , α-Al_2O_3-N_2(TRIS), α-Al_2O_3-PDA-O_2, α-Al_2O_3-O_2, α-Al_2O_3-PDA-O_2(TRIS), α-Al_2O_3-O_2(TRIS), α-Al_2O_3-PDA-O_2(HMTA) and α-Al_2O_3-O_2(HMTA).

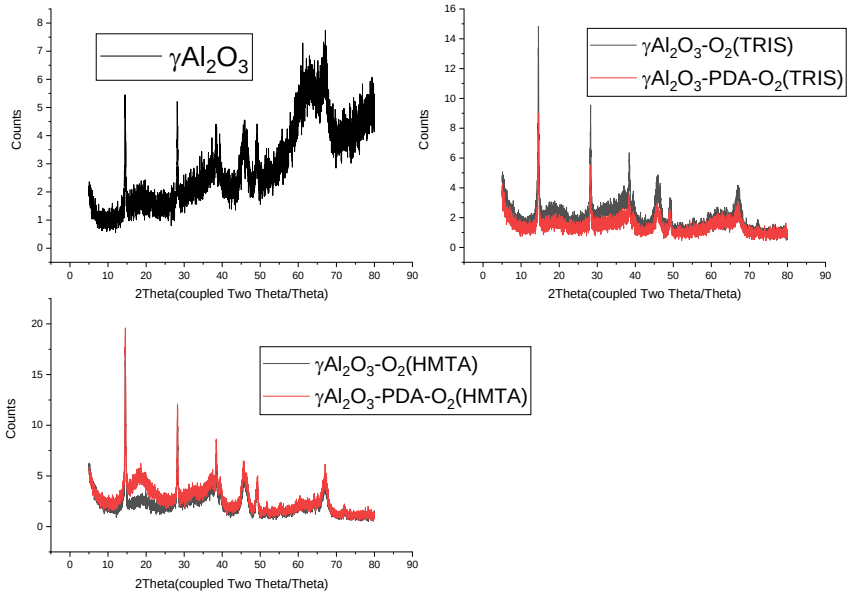

Figure 34: XRD pattern of γ-Al_2O_3 and γ-Al_2O_3-O_2(TRIS) , γ-Al_2O_3-PDA-O_2(TRIS), γ-Al_2O_3-O_2(HMTA) and γ-Al_2O_3-PDA-O_2(HMTA)γ-Al2O3-PDA-O2(TRIS), γ-Al2O3-O2(HMTA) and γ-Al2O3-PDA-O2(HMTA).

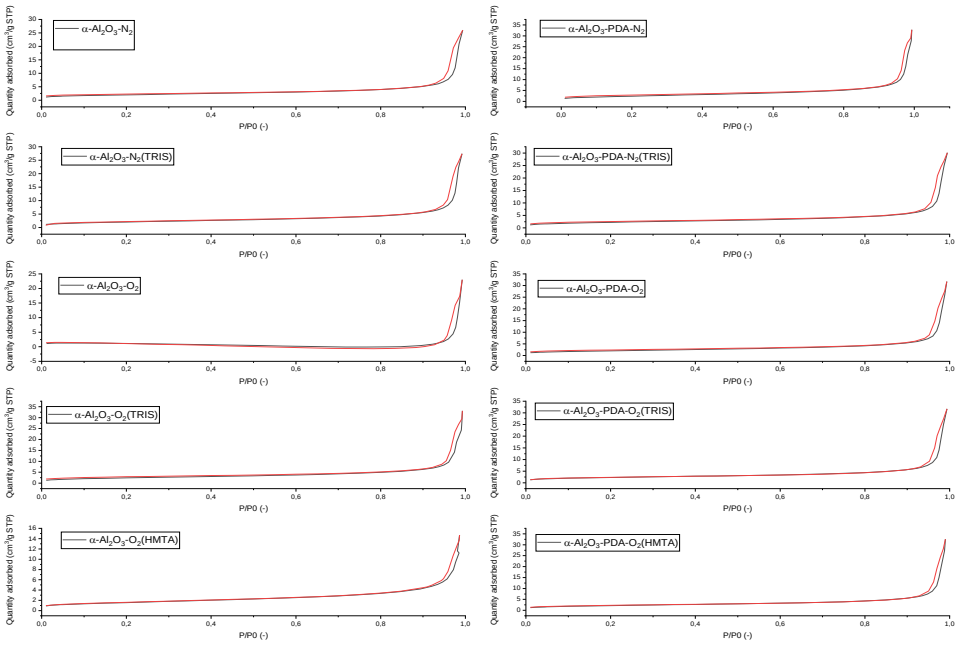

Figure 35: Nitrogen physisorption isotherms of α-Al_2O_3-PDA-N_2, α-Al_2O_3-N_2, α-Al_2O_3-PDA-N_2(TRIS) , α-Al_2O_3-N_2(TRIS), α-Al_2O_3-PDA-O_2, α-Al_2O_3-O_2, α-Al_2O_3-PDA-O_2(TRIS), α-Al_2O_3-O_2(TRIS), α-Al_2O_3-PDA-O_2(HMTA) and α-Al_2O_3-O_2(HMTA).

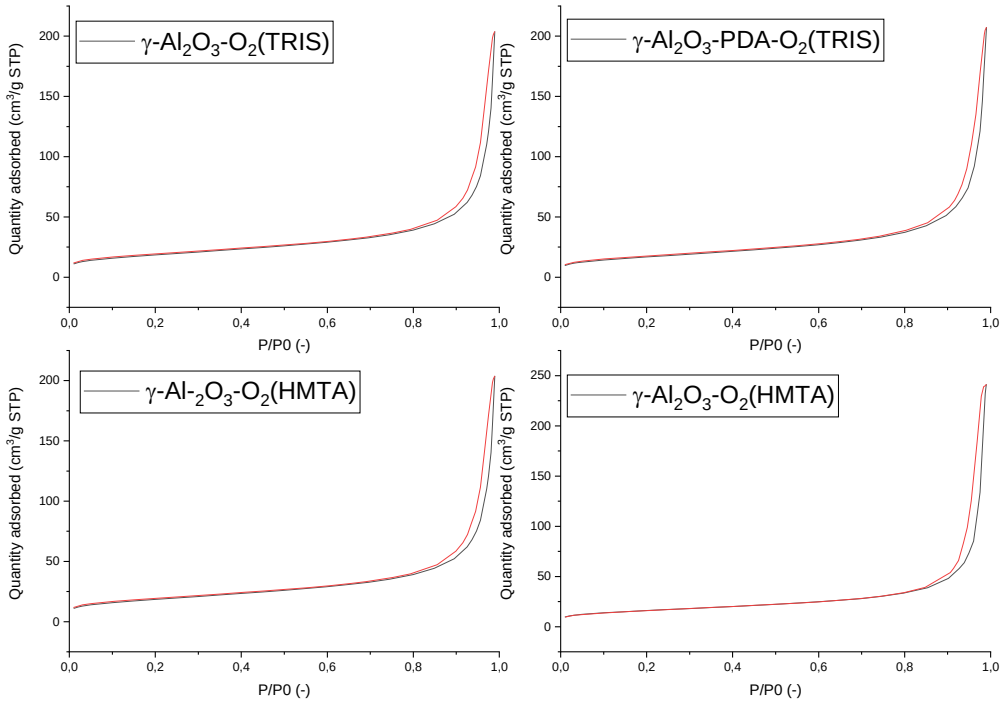

Figure 36: Nitrogen physisorption isotherms of γ-Al_2O_3-O_2(TRIS) , γ-Al_2O_3-PDA-O_2(TRIS), γ-Al_2O_3-O_2(HMTA) and γ-Al_2O_3-PDA-O_2(HTA).

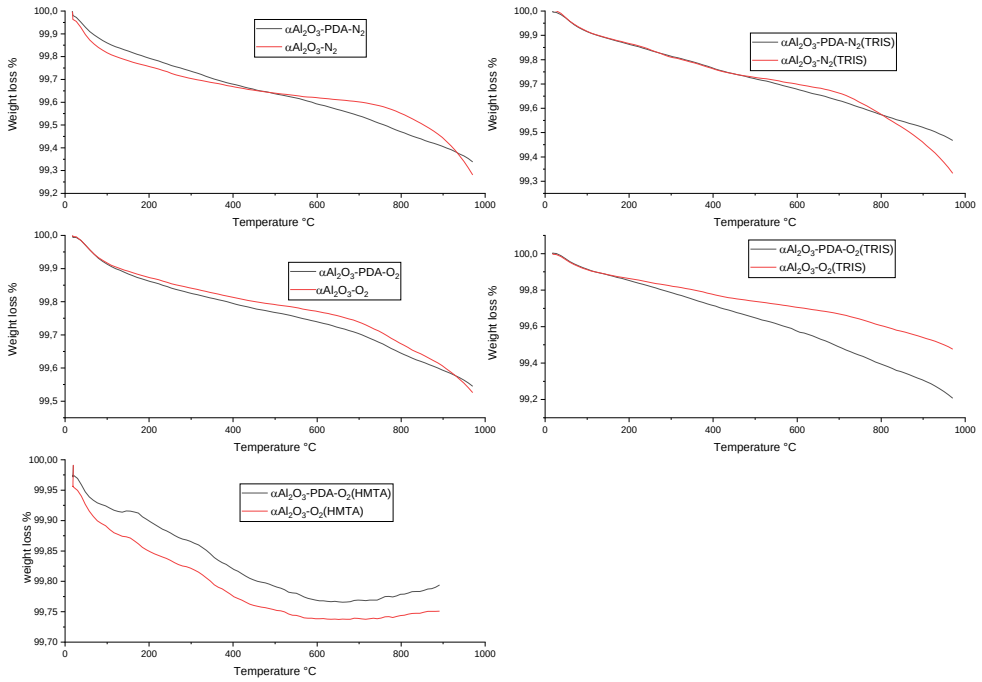

Figure 37: TGA analysis of α-Al_2O_3-PDA-N_2, α-Al_2O_3-N_2, α-Al_2O_3-PDA-N_2(TRIS) , α-Al_2O_3-N_2(TRIS), α-Al_2O_3-PDA-O_2, α-Al_2O_3-O_2, α-Al_2O_3-PDA-O_2(TRIS), α-Al_2O_3-O_2(TRIS), α-Al_2O_3-PDA-O_2(HMTA) and α-Al_2O_3-O_2(HMTA).

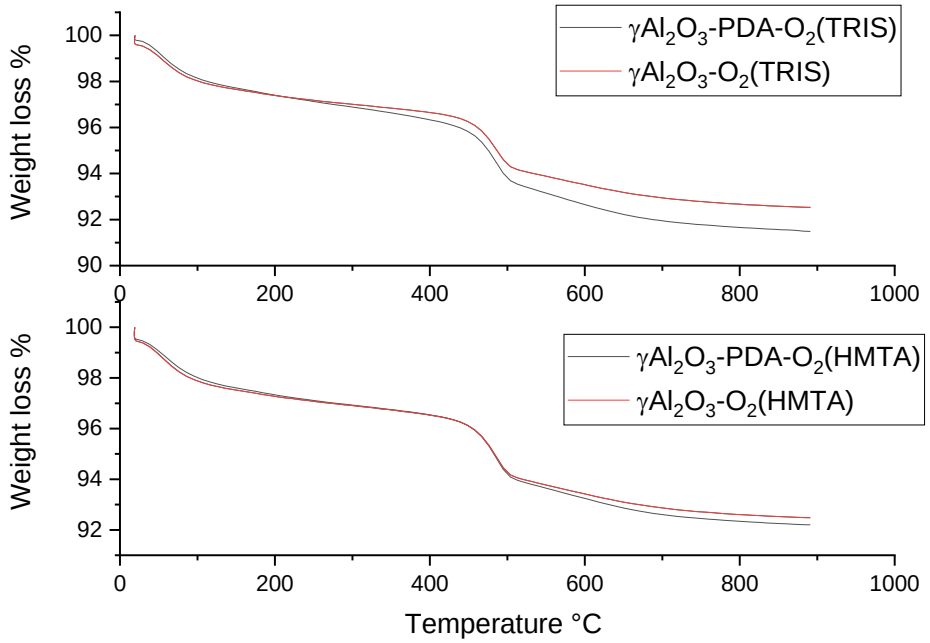

Figure 38: TGA analysis of γ-Al_2O_3-O_2(TRIS) , γ-Al_2O_3-PDA-O_2(TRIS), γ-Al_2O_3-O_2(HMTA) and γ-Al_2O_3-PDA-O_2(HMTA)

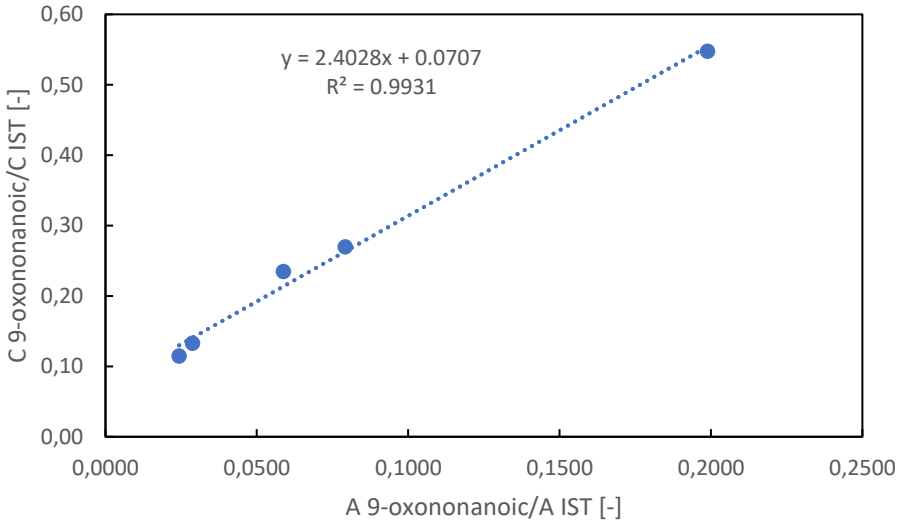
y = 2.4028x + 0.0707
R² = 0.9931
C 9-oxononanoic/C IST [-]
A 9-oxononanoic/A IST [-]
0,60
0,50
0,40
0,30
0,20
0,10
0,00
0,0000
0,0500
0,1000
0,1500
0,2000
0,2500

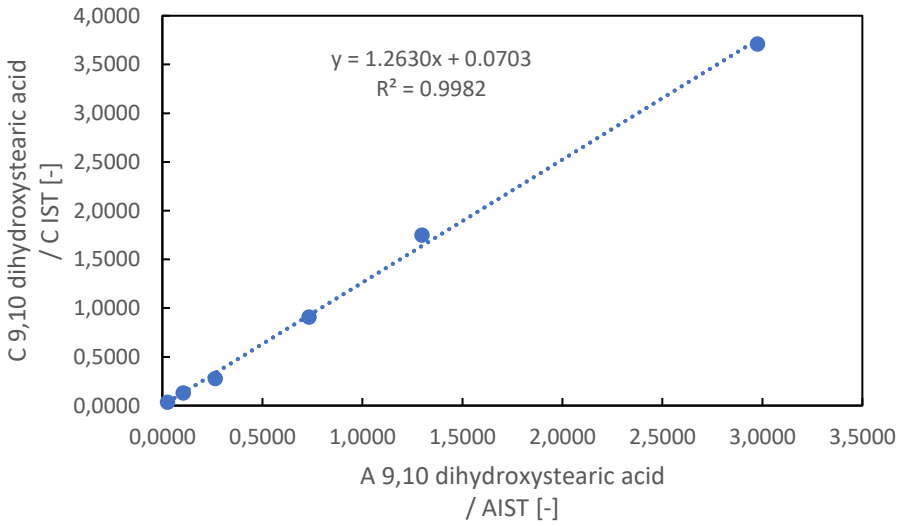
y = 1.2630x + 0.0703
R² = 0.9982
C 9,10 dihydroxystearic acid / C IST [-]
A 9,10 dihydroxystearic acid / AIST [-]
4,0000
3,5000
3,0000
2,5000
2,0000
1,5000
1,0000
0,5000
0,0000
0,0000
0,5000
1,0000
1,5000
2,0000
2,5000
3,0000
3,5000

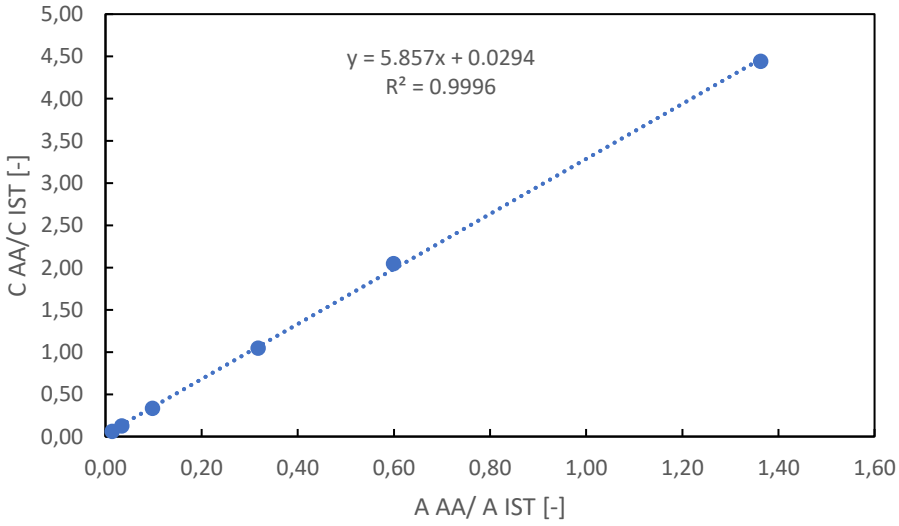
y = 5.857x + 0.0294
R² = 0.9996
C AA/C IST [-]
A AA/ A IST [-]
5,00
4,50
4,00
3,50
3,00
2,50
2,00
1,50
1,00
0,50
0,00
0,00
0,20
0,40
0,60
0,80
1,00
1,20
1,40
1,60

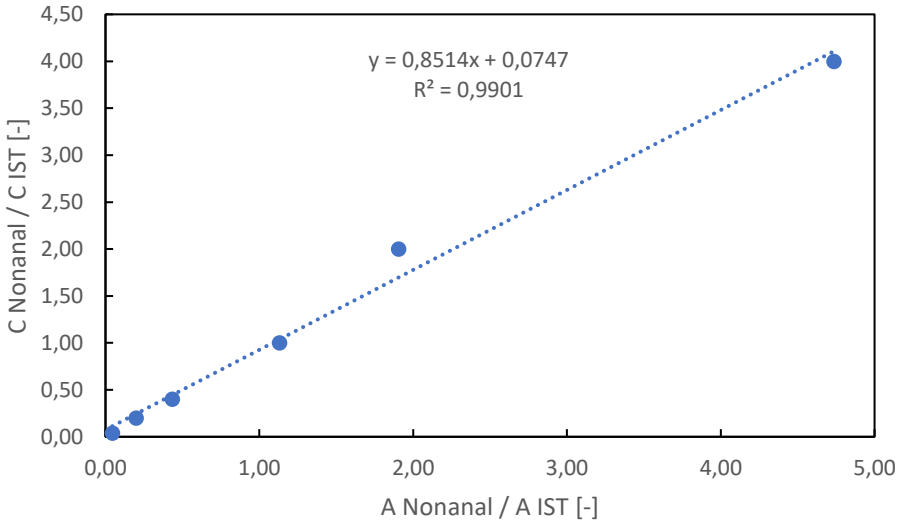
y = 0,8514x + 0,0747
R² = 0,9901
C Nonanal / C IST [-]
A Nonanal / A IST [-]
4,50
4,00
3,50
3,00
2,50
2,00
1,50
1,00
0,50
0,00
0,00
1,00
2,00
3,00
4,00
5,00

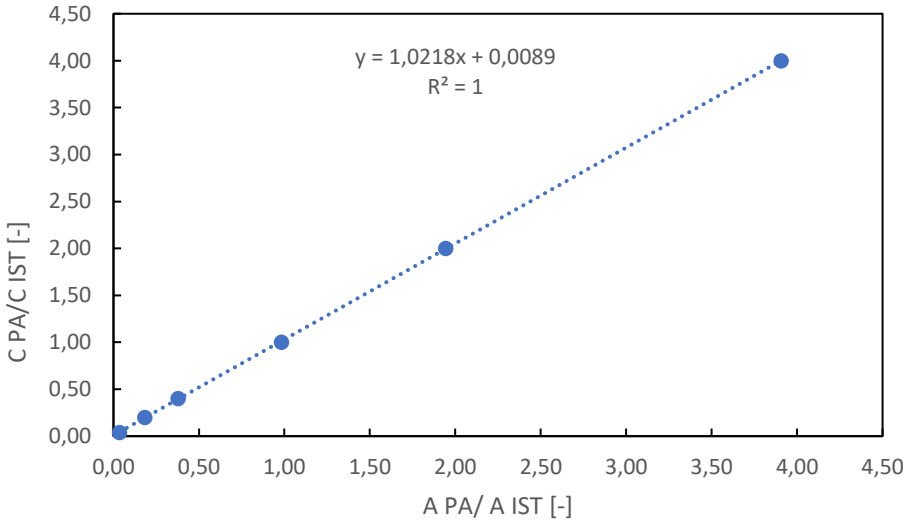
y = 1,0218x + 0,0089
R² = 1
C PA/C IST [-]
A PA/ A IST [-]
4,50
4,00
3,50
3,00
2,50
2,00
1,50
1,00
0,50
0,00
0,00
0,50
1,00
1,50
2,00
2,50
3,00
3,50
4,00
4,50

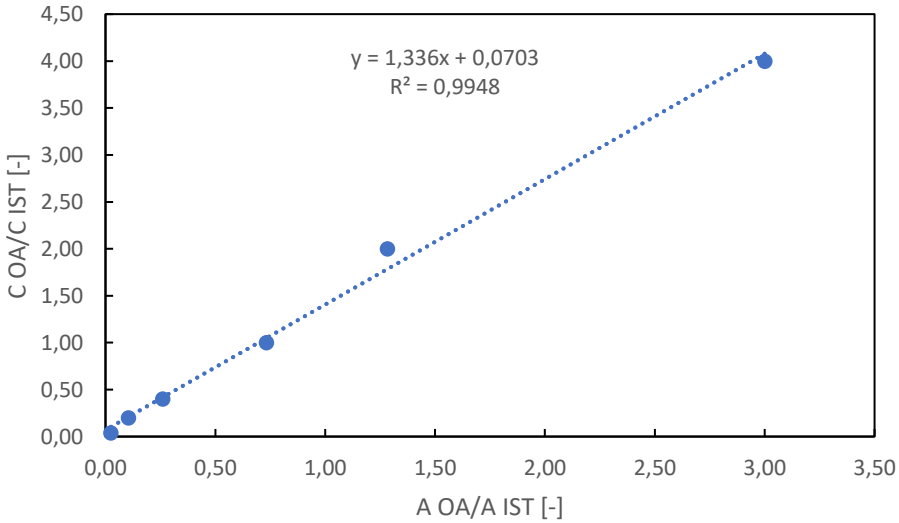
y = 1,336x + 0,0703
R² = 0,9948
C OA/C IST [-]
A OA/A IST [-]
4,50
4,00
3,50
3,00
2,50
2,00
1,50
1,00
0,50
0,00
0,00
0,50
1,00
1,50
2,00
2,50
3,00
3,50

Oxidative cleavage of oleic acid with alumina-ruthenium composites

Presented by Odile Malburny

In a near future, the world will have to face the shortage of petrochemical molecules which are currently the most important raw material for the chemical industry. In addition to the scarcity which leads to economic concern, the pollution that arises from petroleum materials is also a big concern. Therefore, a lot of effort has been paid to find new renewable, biodegradable, harmless feedstocks which can replaced petrochemical molecules. Oils and fats have similar structure as petrochemical molecules and are abundant in the nature which makes them promising as new renewable feedstocks. Oleochemistry is the process by which vegetable oils and animal fats are transformed into value-added products. Lipids are built from triglycerides. The decomposition of these triglycerides will produce fatty acids (FA), either saturated (without carbon-carbon double bond) or unsaturated (with carbon-carbon double bond) ones.

Oleic acid (OA) is the most abundant mono-unsaturated fatty acid (UFA) present in Nature. OA is currently used industrially to produce azelaic acid (AA) and pelargonic acid (PA). AA is a linear saturated dicarboxylic acid with 9 carbons. AA is used in pharmaceutical, cosmetic and polymers industry and can also serve as a lubricant or as a plasticizer. In addition, the market price of AA is expected to reach 140m USD by 2025. PA is mainly used in pesticides and herbicides. The production of PA and AA is usually performed via ozonolysis of OA, the oxidative cleavage of the double carbon bond is done with O_3 as oxidant agent. On the other hand, the use of ozone present safety risk and pollution issues. Despite the issue of using ozone, the alternative of heterogeneous catalysts for the oxidative cleavage of UFA's are poorly documented.

In this work, a novel Ru heterogeneous composite catalyst for the oxidative cleavage of oleic was synthesized. As a matter of fact, Ru in its oxidation state +VIII (RuO_4) can perform the oxidative cleavage of OA into PA and AA, at room temperature and atmospheric pressure. Alumina was used as support and polydopamine was used as an anchoring system for the complexion of Ru ions. The best catalyst resulted to be active in the oxidative cleavage of oleic acid reaching conversion of 98% after 7 hours and retains its activity during 4 recycles with high selectivity towards PA and AA.

During this work, the benefit of PDA has been clearly demonstrated. However, the interactions between PDA and the alumina, and between PDA and ruthenium, remain unclear and would deserve to be further examined.

UNIVERSITÉ CATHOLIQUE DE LOUVAIN
Faculté des bioingénieurs
Croix du Sud, 2 bte L7.05.01, 1348 Louvain-la-Neuve, Belgique | **www.uclouvain.be/agro**